

---

# On the Burden of Achieving Fairness in Conformal Prediction

---

**Ziang Gao**\*<sup>†</sup>  
 McGill University  
 Montreal, Canada  
 ziang.gao@mail.mcgill.ca

**Pengqi Liu**\*  
 McGill University  
 Montreal, Canada  
 pengqi.liu@mail.mcgill.ca

**Archer Yi Yang**  
 McGill University  
 Montreal, Canada  
 archer.yang@mcgill.ca

**Mouloud Belbahri**  
 TD Insurance  
 Montreal, Canada  
 mouloud.belbahri@td.com

**Jesse C. Cresswell**  
 Layer 6 AI  
 Toronto, Canada  
 jesse@layer6.ai

**Masoud Asgharian**  
 McGill University  
 Montreal, Canada  
 masoud.asgharian2@mcgill.ca

## Abstract

Conformal prediction is often calibrated with a single pooled threshold, but this can hide cross-group heterogeneity in score distributions and distort group-wise coverage. We study this phenomenon through the population score distributions underlying split conformal calibration. First, we derive a conservation law and lower bound showing that pooled calibration incurs irreducible group-wise coverage distortion at a scale set by cross-group quantile heterogeneity. Second, we demonstrate that the two leading fairness definitions for conformal prediction, Equalized Coverage and Equalized Set Size, are fundamentally in tension. Third, we quantify the cost of moving between policies which treat groups separately or pool them. Experiments on synthetic and real data confirm the same bidirectional trade-off after finite-sample calibration. Our results show that, for the policy families studied here, calibration choice does not remove cross-group heterogeneity; it determines whether the resulting distortion appears in the coverage or size dimension, providing a principled lens for analyzing fairness-oriented calibration choices in practice.

## 1 Introduction

Conformal prediction (CP) [27, 22] provides a model-agnostic solution for quantifying uncertainty over machine learning predictions. Let  $Y$  be the outcome variable and  $X \in \mathbb{R}^p$  be a vector of features. Given a calibration dataset  $\{(X_i, Y_i)\}_{i=1}^n$ , CP generates *prediction sets*  $\hat{C}(X_{n+1})$  for test label  $Y_{n+1}$ , with a *coverage* guarantee that the true label is in the set with user-specified probability  $1 - \alpha$  for  $\alpha \in (0, 1)$ , i.e.,  $\mathbb{P}(Y_{n+1} \in \hat{C}(X_{n+1})) \geq 1 - \alpha$ . Smaller sets indicate less uncertainty about the prediction for  $Y_{n+1}$ , so average set size is commonly used as a metric given a fixed coverage level  $1 - \alpha$ . CP is extremely versatile in applications since the coverage guarantee is valid in finite samples and is distribution-free, assuming only that test data is exchangeable with the calibration dataset.

CP is often implemented with a single threshold calibrated on the pooled calibration set. This delivers marginal coverage over the entire distribution, but still allows some groups within the data to be under-covered if others are over-covered to compensate. Exact distribution-free conditional coverage is impossible in general [8]. We therefore study group-conditional CP as an intermediate target. Group-wise calibration resolves the potential disparity in coverage relative to pooled calibration [26],

---

\*Equal contribution. Alphabetically ordered by last name.

<sup>†</sup>Corresponding author. Email: ziang.gao@mail.mcgill.ca.

but the same heterogeneity reappears as disparity in expected set size. Thus, a calibration policy does not remove heterogeneity; it determines whether the disparity appears in coverage or in set size.

In this work, we present a theoretical and empirical study of the fundamental tension between coverage disparity and set size disparity when applying CP over data containing heterogeneous groups. Our theoretical results give practitioners a principled way to understand what is gained and what is sacrificed when one fairness-oriented calibration objective is chosen over another. We study this question through the population score distributions underlying split conformal prediction. This viewpoint separates the structural effect of group heterogeneity from finite-sample calibration noise.

Our contributions are as follows:

- We characterize pooled conformal calibration through a conservation law and lower bound for group-wise coverage, showing that pooled calibration can hide nontrivial group-level distortion.
- We establish a bidirectional impossibility result showing that *exact group-wise coverage and equalized expected set size cannot, in general, be achieved simultaneously*. This identifies a structural limitation of fairness-oriented conformal calibration policies.
- We quantify the costs of switching from pooled calibration to group-wise calibration, and from the coverage-calibrated setting to equalized-size calibration.

The rest of the paper is organized as follows. Section 2 reviews related work. Sections 3 and 4 develop our theoretical results. Section 5 translates the theory into empirical results on synthetic and real datasets. Section 6 concludes with limitations and future directions. Technical discussions, supplemental results, proofs, and additional experimental details are deferred to the appendices.

## 2 Related Work

A central line of work studies fairness notions for CP. **Equalized Coverage** [20] identifies unequal group-wise empirical coverage under pooled calibration as a fairness concern, and later work extends this perspective to adaptively selected groups and more general frameworks [30, 25]. Other works extend additional fairness notions to conformal prediction, including demographic parity [17], equal opportunity [28], and counterfactual fairness criteria [12]. A related literature studies fairness in downstream decision-making, where conformal sets are provided as a decision aid: conformal sets can improve human decisions [4], but human-subject experiments show that enforcing Equalized Coverage can worsen downstream fairness whereas **Equalized Set Size** can improve it [5]; Liu et al. [18] extend this perspective with an LLM-in-the-loop evaluator. Tasar [24] studies a trade-off between coverage parity and deferral parity in a binary human-in-the-loop setting. Our work is complementary to this literature: we formalize a structural incompatibility between Equalized Coverage and Equalized Set Size, and provide practitioners with a clear lens for weighing the costs of these disparities. The closest conceptual precedent to our results is the classical algorithmic-fairness literature on scores and classifiers: Hardt et al. [14] introduce equalized odds and equal opportunity; Chouldechova [3] and Kleinberg et al. [15] establish impossibility results for competing fairness criteria under unequal base rates; Lazar Reich and Vijaykumar [16] identify settings where partial reconciliation is possible. Our work identifies analogous impossibility results in CP, where the structural driver comes from cross-group heterogeneity in conformal quantiles. More broadly, our work is also related to limits of conditional coverage [8, 11] and efficiency-oriented work on volume optimality for structured prediction sets [10] and learned size-coverage trade-offs [2], but differs in isolating how cross-group heterogeneity constrains the simultaneous attainment of two group-level calibration objectives: exact group-wise coverage and equalized expected set size.

## 3 Pooled Calibration and Groupwise Coverage Distortion

This section is organized around two questions. What does a single pooled threshold guarantee? How large is the resulting group-wise coverage distortion when group-specific quantiles differ? We first recall the finite-sample CP constructions to fix notation, then introduce the population-level objects that help answer these questions.

### 3.1 Conformal Prediction

We work in the standard setting of split conformal prediction [22]. Let  $X \in \mathbb{R}^p$  be a covariate vector,  $Y$  be a label, and  $S(X, Y)$  be a nonconformity score. Given a calibration sample  $\mathcal{D}_{\text{cal}} = \{(X_i, Y_i)\}_{i=1}^n$ , let  $S_i = S(X_i, Y_i)$  for  $i = 1, \dots, n$  denote the calibration scores. Pooled split CP

computes an empirical quantile at level  $1 - \alpha$  over the entire calibration sample as

$$\hat{q} := \text{Quantile}(1 - \alpha; \{S_i\}_{i=1}^n \cup \{\infty\}) \quad (1)$$

where the (pooled) quantile is equivalently the  $\lceil (n+1)(1-\alpha) \rceil$ -th order statistic of the augmented multiset. For any threshold  $t$ , we define the associated prediction set as the collection of labels whose scores fall below the threshold

$$\widehat{C}_t(X_{n+1}) := \{y : S(X_{n+1}, y) \leq t\}. \quad (2)$$

The CP set for a new test point is thus given by  $\widehat{C}_{\hat{q}}(X_{n+1})$ , which, under exchangeability of the calibration and test examples, has the marginal coverage guarantee  $\mathbb{P}(Y_{n+1} \in \widehat{C}_{\hat{q}}(X_{n+1})) \geq 1 - \alpha$ .

On the other hand, to construct a prediction set with a group-wise coverage guarantee [26], we define  $G : \mathcal{X} \rightarrow \mathcal{G} = \{1, \dots, K\}$  to be a prespecified discrete partition of the covariate space, with group label  $G(X) = g$ , and choose threshold  $t$  in Equation (2) to be the  $1 - \alpha$  quantile (group-wise) of calibration scores within group  $g$ , i.e.  $\hat{q}_g := \text{Quantile}(1 - \alpha; \{S_i\}_{i:G(X_i)=g} \cup \{\infty\})$ . The prediction set  $\widehat{C}_{\hat{q}_g}(X_{n+1})$ , under exchangeability within each prespecified group, satisfies  $\mathbb{P}\{Y_{n+1} \in \widehat{C}_{\hat{q}_g}(X_{n+1}) \mid G(X_{n+1}) = g\} \geq 1 - \alpha$  for a test point in group  $g$ .

### 3.2 Conservation Law for the Pooled Threshold

We first investigate the group-wise miscoverage of a marginal prediction set. The standard split CP set  $\widehat{C}_{\hat{q}}(X)$  with the pooled empirical quantile  $\hat{q}$  only has a marginal coverage guarantee rather than a group-wise one: some groups may be under-covered while others are over-covered. To study the group-wise miscoverage of  $\widehat{C}_{\hat{q}}(X)$ , we define the *signed group-wise coverage distortion* for a test point in group  $g$  by

$$\varepsilon_g(\hat{q}) := \mathbb{P}\{Y \in \widehat{C}_{\hat{q}}(X) \mid G(X) = g\} - (1 - \alpha). \quad (3)$$

A positive  $\varepsilon_g(\hat{q})$  corresponds to over-coverage in group  $g$ , while a negative value corresponds to under-coverage. Under standard quantile-consistency conditions, the empirical pooled quantile  $\hat{q}$  concentrates around the pooled population quantile  $q$  of the nonconformity score  $S$ :

$$q := \inf\{t \in \mathbb{R} : F_S(t) \geq 1 - \alpha\} \quad (4)$$

with  $F_S(t) = \mathbb{P}(S \leq t)$ . For any fixed threshold  $t$ , we can see that the group-wise coverage is the conditional CDF of the nonconformity score  $S$ :

$$\mathbb{P}\{Y \in \widehat{C}_t(X) \mid G(X) = g\} = \mathbb{P}\{S \leq t \mid G(X) = g\} =: F_{S|g}(t). \quad (5)$$

In the large calibration sample case,  $\varepsilon_g(\hat{q})$  can be approximated by the *population signed group-wise coverage distortion*  $\varepsilon_g(q)$ , defined as:

$$\varepsilon_g(q) := F_{S|g}(q) - (1 - \alpha). \quad (6)$$

We begin by characterizing what the pooled threshold  $q$  guarantees at the aggregate level for  $\varepsilon_g(q)$ . By definition of  $q$  (Equation (4)), Theorem 1 below gives the aggregate identity for group-wise coverage distortion; when  $F_S$  is continuous at  $q$ , this identity becomes a zero-sum conservation law. (All proofs are presented in Appendix B.)

**Theorem 1.** (*Conservation law for pooled calibration*) Let  $p_g := \mathbb{P}\{G(X) = g\}$  be the group mass. Group-wise coverage distortion  $\varepsilon_g(q)$  under the pooled threshold satisfies the aggregate identity

$$\sum_{g \in \mathcal{G}} p_g \varepsilon_g(q) = F_S(q) - (1 - \alpha) =: \delta(q). \quad (7)$$

If  $F_S$  is continuous at  $q$ , then  $\delta(q) = 0$ , and hence  $\sum_{g \in \mathcal{G}} p_g \varepsilon_g(q) = 0$ .

**Remark 1.** If  $F_S$  has a jump at  $q$ , randomized tie handling via the probability integral transform restores the zero-sum identity. Let  $U \sim \text{Uniform}(0, 1)$  be independent of  $S$  and  $G$ , and define  $Z := F_S(S^-) + U \cdot (F_S(S) - F_S(S^-))$ . Then  $Z \sim \text{Uniform}(0, 1)$ , which means that the event  $\{Z \leq 1 - \alpha\}$  implements randomized tie handling at  $q$ . Next, we define  $\tilde{\varepsilon}_g := \mathbb{P}(Z \leq 1 - \alpha \mid G = g) - (1 - \alpha)$  to obtain  $\sum_{g \in \mathcal{G}} p_g \tilde{\varepsilon}_g = 0$ .

**Take-away.** A pooled threshold  $q$  can satisfy marginal coverage while miscovering individual groups, which can be a fairness concern. Under continuity, or under randomized tie handling in the atomic case, Theorem 1 shows that weighted over-coverage in some groups is exactly balanced by weighted under-coverage in others.

Theorem 1 is an additive form. A product-type form of the conservation law is given in Appendix A.1.

### 3.3 The Pooled Threshold Uncertainty Relation

We now move from balance to magnitude. For each group, let  $q_g := \inf\{t \in \mathbb{R} : F_{S|g}(t) \geq 1 - \alpha\}$  denote the population group quantile. We quantify the irreducible root mean square (RMS) group-wise miscoverage induced by using a pooled threshold in the presence of group-quantile heterogeneity.

**Assumption 1.** There exists a common  $\eta > 0$  such that, for each  $g \in \mathcal{G}$ , the conditional CDF  $F_{S|g}$  is absolutely continuous on the interval  $I_g := [\min(q, q_g) - \eta, \max(q, q_g) + \eta]$ , with density  $f_{S|g}$  satisfying  $f_{S|g}(t) > 0$  for almost every  $t \in I_g$ . Moreover, whenever  $q \neq q_g$ ,  $\text{ess inf}_{t \in J_g} f_{S|g}(t) > 0$ , where  $J_g := [\min(q, q_g), \max(q, q_g)]$ . In particular,

$$m_g(q) := \text{ess inf}_{t \in J_g} f_{S|g}(t), \quad (8)$$

with the convention  $m_g(q) = 0$  when  $q = q_g$ .

Let  $q_G$  and  $\varepsilon_G(q)$  denote the random variable versions of  $q_g$  and  $\varepsilon_g(q)$ , respectively, and

$$F_{S|g}(q) - F_{S|g}(q_g) = \int_{q_g}^q f_{S|g}(t) dt. \quad (9)$$

**Definition 1.** The *effective stiffness* is defined as

$$m_{\text{eff}}(q) := \sqrt{\frac{\mathbb{E}[m_G(q)^2 (q - q_G)^2]}{\mathbb{E}[(q - q_G)^2]}} \quad \text{whenever } \mathbb{E}[(q - q_G)^2] > 0. \quad (10)$$

Let

$$\sigma_\Delta^2 := \text{Var}(q_G) = \mathbb{E}[(q_G - \mathbb{E}[q_G])^2] = \sum_{g \in \mathcal{G}} p_g (q_g - \sum_{g' \in \mathcal{G}} p_{g'} q_{g'})^2. \quad (11)$$

The quantity  $\sigma_\Delta$  measures the cross-group dispersion of the target quantiles  $\{q_g\}$ . When  $\sigma_\Delta = 0$ , pooled and group-conditional calibration coincide at the population level. As a property of the population and choice of nonconformity score,  $\sigma_\Delta$ , which we refer to as *intrinsic heterogeneity*, is a central object in our study of the differences between pooled and group-wise conformal calibration.

**Theorem 2.** (*Pooled-threshold uncertainty relation*) Suppose Assumption 1 holds. Then

$$\text{Var}(\varepsilon_G(q)) \geq m_{\text{eff}}(q)^2 \text{Var}(q_G). \quad (12)$$

**Take-away.** Under pooled calibration, the cross-group variation in the target quantiles induces a non-zero cross-group disparity in group-wise coverage distortions at the scale  $m_{\text{eff}}(q)\sigma_\Delta$ .

Thus, the fact that a pooled threshold causes group-wise coverage distortion is not an artifact of finite-sample calibration noise, but is already present at the population level.

## 4 Calibration Policies and Coverage–Size Trade-offs

### 4.1 Equalized Coverage versus Equalized Expected Set Size

The results above quantify the irreducible coverage error incurred by a single pooled threshold  $q$ . We now ask what happens when one changes the calibration policy to mitigate pooled threshold distortion. We formalize two directions of the resulting trade-off between two group-level fairness criteria: *Equalized Coverage* [20], meaning  $\mathbb{P}(S \leq t_g \mid G = g) = 1 - \alpha$  for all  $g$ , and *Equalized Expected Set Size* [4], meaning the expected size of the CP set under a group-specific threshold  $t_g$  is equal to a constant  $\lambda$ , i.e.  $\mathbb{E}[|\widehat{C}_{t_g}(X)| \mid G = g] = \lambda$  for all  $g$ .

Recall that, for each group  $g \in \mathcal{G}$ , the threshold  $q_g := F_{S|g}^{-1}(1 - \alpha)$  achieves exact group-wise coverage level  $1 - \alpha$  whenever  $F_{S|g}$  is continuous (Equation (5)). We first present one sufficient condition, going from equalized coverage to expected-size disparity. To do so, fix a reference group  $r \in \mathcal{G}$  and define  $\mathcal{H}_r := \{g \in \mathcal{G} : q_g \geq q_r\}$ , the set of groups whose coverage-calibrated thresholds are at least as large as that of the chosen reference group. Let  $\ell_g(t) := \mathbb{E}[|\widehat{C}_t(X)| \mid G = g]$  be the group-wise expected size of the CP set at threshold  $t$ . For a reference group  $r$ , define the restricted mean squared size gap

$$D_r^2 := \mathbb{E}[(\ell_G(q_G) - \ell_r(q_r))^2 \mathbf{1}\{G \in \mathcal{H}_r \setminus \{r\}\}]. \quad (13)$$

**Assumption 2.** There exists a reference group  $r \in \mathcal{G}$  with  $\mathcal{H}_r \setminus \{r\} \neq \emptyset$ , and positive constants  $\{c_g\}_{g \in \mathcal{H}_r \setminus \{r\}}$ , such that  $\ell_g(q_r) - \ell_r(q_r) \geq c_g$  for every  $g \in \mathcal{H}_r \setminus \{r\}$ .

Assumption 2 requires that groups that require larger coverage-calibrated thresholds already have larger expected set sizes at a common reference threshold. This gives a sufficient route from equalized coverage to nonzero expected set size disparity across groups.

Theorem 3 below illustrates that equalizing coverage transmits heterogeneity into the size dimension. Under Assumption 2, if groups requiring larger coverage-calibrated thresholds already have larger expected set sizes at the reference threshold, exact group-wise coverage preserves set size disparity.

**Theorem 3.** (*Equalized coverage induces cross-group expected set size disparity*) Assume the score CDF  $F_{S|g}$  is continuous and the map  $t \mapsto \ell_g(t)$  is non-decreasing for all  $g \in \mathcal{G}$ . Suppose Assumption 2 holds for some reference group  $r \in \mathcal{G}$ . Then,

1. The group-wise thresholds  $\{q_g\}_{g \in \mathcal{G}}$ , which achieve an exact group-wise coverage level  $1 - \alpha$ , necessarily induce a nonzero cross-group disparity in expected set size. More precisely, for every  $g \in \mathcal{H}_r \setminus \{r\}$ ,  $\ell_g(q_g) - \ell_r(q_r) \geq c_g > 0$ .  
Consequently,

$$\max_{g, g' \in \mathcal{G}} |\ell_g(q_g) - \ell_{g'}(q_{g'})| \geq \max_{g \in \mathcal{H}_r \setminus \{r\}} c_g > 0. \quad (14)$$

Therefore, exact group-wise coverage cannot simultaneously satisfy equalized expected set size across groups.

2. The restricted mean squared cross-group size disparity relative to the reference group  $r$  satisfies

$$D_r^2 = \sum_{g \in \mathcal{H}_r \setminus \{r\}} p_g (\ell_g(q_g) - \ell_r(q_r))^2 \geq \sum_{g \in \mathcal{H}_r \setminus \{r\}} p_g c_g^2 > 0. \quad (15)$$

**Take-away.** Exact group-wise coverage generally entails unequal expected set sizes across groups.

We now turn to the reverse direction and consider an equalized expected set size policy at target level  $\lambda$ . We define  $\lambda_g := \ell_g(q_g)$ ,  $g \in \mathcal{G}$ , the coverage-calibrated expected set size of group  $g$ , and we denote  $\lambda_G$  as the random-group version of  $\lambda_g$ . We ask how an equalized-size policy alters group-wise coverage. Let  $\tau_g$  denote a group-specific threshold satisfying  $\ell_g(\tau_g) = \lambda$ . That is,  $\tau_g$  is the threshold required for group  $g$  to attain the equalized-size target. To quantify the coverage effect of moving from  $q_g$  to  $\tau_g$ , we impose local regularity only on the segment between  $q_g$  and  $\tau_g$ .

**Assumption 3.** (Local regularity for equalized-size perturbations) For each group  $g$ , on the segment between  $q_g$  and  $\tau_g$  both  $F_{S|g}$  and  $\ell_g$  are absolutely continuous, with  $\ell_g$  non-decreasing, derivatives satisfying  $f_{S|g}(t) \geq m_g > 0$ ,  $|\ell'_g(t)| \leq V_g$  for almost every  $t$  on the segment, where  $0 < V_g < \infty$ .

Theorem 4 below establishes the reverse direction of the trade-off compared to Theorem 3. Under an equalized-size policy  $\{\tau_g\}_{g \in \mathcal{G}}$ , one may eliminate cross-group disparity in expected set size, but only at the expense of introducing cross-group disparity in coverage whenever the common target level  $\lambda$  lies strictly between two distinct coverage-calibrated set sizes. We utilize the local coverage–size conversion factor  $\kappa_g := m_g/V_g$  for each group  $g$ .

**Theorem 4.** (*Equalized expected set size induces cross-group coverage disparity*) Suppose Assumption 3 holds, and suppose for some common target level  $\lambda$  the thresholds  $\{\tau_g\}_{g \in \mathcal{G}}$  satisfy  $\ell_g(\tau_g) = \lambda$ ,  $g \in \mathcal{G}$ . Then the following results hold.

(i) For every group  $g$  with  $\lambda_g < \lambda$ ,  $F_{S|g}(\tau_g) - (1 - \alpha) \geq \kappa_g (\lambda - \lambda_g)$ .

(ii) For every group  $g'$  with  $\lambda_{g'} > \lambda$ ,  $(1 - \alpha) - F_{S|g'}(\tau_{g'}) \geq \kappa_{g'} (\lambda_{g'} - \lambda)$ .

Consequently, for any pair  $g, g' \in \mathcal{G}$  such that  $\lambda_g < \lambda < \lambda_{g'}$ , we have the pairwise lower bound

$$F_{S|g}(\tau_g) - F_{S|g'}(\tau_{g'}) \geq \kappa_g (\lambda - \lambda_g) + \kappa_{g'} (\lambda_{g'} - \lambda). \quad (16)$$

In particular, if there exist groups  $g, g'$  with  $\lambda_g < \lambda_{g'}$  and  $\lambda \in (\lambda_g, \lambda_{g'})$ , then

$$\max_{a, b \in \mathcal{G}} |F_{S|a}(\tau_a) - F_{S|b}(\tau_b)| \geq \kappa_g (\lambda - \lambda_g) + \kappa_{g'} (\lambda_{g'} - \lambda) > 0. \quad (17)$$

**Take-away.** Whenever the equalized-size level  $\lambda$  lies strictly between two distinct coverage-calibrated set sizes, the equalized set size policy induces nonzero coverage disparity.

Together, Theorem 3 and Theorem 4 show that **the two leading fairness notions in CP, namely Equalized Coverage and Equalized Set Size, cannot in general be achieved simultaneously**. To the best of our knowledge, this is the first formal result in CP establishing this structural incompatibility. This places our result alongside the classical impossibility theorems of Kleinberg et al. [15] and Chouldechova [3], but in the distinct setting of CP, where the trade-off is driven by cross-group heterogeneity in conformal quantiles and its effect on coverage and set size. We next quantify the scale of policy-conversion distortions.

## 4.2 Quantitative Bounds for Policy-Conversion Distortions

We now turn from directional trade-off results to quantitative policy-conversion bounds. The goal is to measure the scale of the distortions induced when one moves between pooled calibration, exact group-wise coverage, and equalized-size calibration. We first quantify the cost of moving from pooled calibration to exact group-wise coverage. To do so, we require a local responsiveness condition on the group-wise size curves along the segment between  $q$  and  $q_g$ .

**Assumption 4.** (Local set size responsiveness for group-wise calibration) For each group  $g$ , the mapping  $t \mapsto \ell_g(t)$  is absolutely continuous on the segment between  $q$  and  $q_g$ , and is non-decreasing on the segment. Moreover, its derivative  $\ell'_g(t)$  is defined almost everywhere and satisfies  $\ell'_g(t) \geq v_g > 0$  for almost every  $t$  on that segment.

Next, we define the *effective set-size responsiveness* as

$$v_{\text{eff}}(q) := \sqrt{\frac{\mathbb{E}[v_G^2 (q - q_G)^2]}{\mathbb{E}[(q - q_G)^2]}} \quad \text{whenever } \mathbb{E}[(q - q_G)^2] > 0. \quad (18)$$

The next corollary converts the intrinsic heterogeneity  $\sigma_\Delta$  into a lower bound on set size distortion.

**Corollary 1.** (Exact group-wise coverage induces set size distortion) Suppose Assumption 4 holds. Let the pooled threshold  $q$  be replaced by the group-wise thresholds  $\{q_g\}$ . Then the RMS set size lower bound is

$$\sqrt{\mathbb{E}[(\ell_G(q_G) - \ell_G(q))^2]} \geq v_{\text{eff}}(q) \sigma_\Delta. \quad (19)$$

**Take-away.** Exact group-wise coverage generally incurs a measurable expected set size distortion.

Corollary 1 turns the directional statement into a scale statement. It shows that moving from pooled calibration to exact group-wise coverage produces a set size change with magnitude controlled by the same underlying cross-group quantile distortion.

We next quantify the reverse conversion cost. Theorem 4 establishes the reverse direction of the trade-off by showing that an equalized-size policy induces coverage disparity. The following corollary converts the same argument into an aggregate RMS lower bound by measuring how far the equalized-size thresholds  $\{\tau_g\}$  shift coverage from the exact group-wise benchmark  $\{q_g\}$ . From Theorem 4, we obtain  $\mathbb{E}[(F_{S|G}(\tau_G) - F_{S|G}(q_G))^2] \geq \mathbb{E}[\kappa_G^2 (\lambda_G - \lambda)^2]$ ,  $\kappa_G := m_G/V_G$ . Before we formally state this result, we define the *effective coverage responsiveness*

$$\kappa_{\text{eff}}(\lambda) := \sqrt{\frac{\mathbb{E}[(m_G/V_G)^2 (\lambda - \lambda_G)^2]}{\mathbb{E}[(\lambda - \lambda_G)^2]}} \quad \text{whenever } \mathbb{E}[(\lambda - \lambda_G)^2] > 0, \quad (20)$$

and the set-size heterogeneity  $\sigma_\lambda := \text{sd}(\lambda_G) = \sqrt{\text{Var}(\lambda_G)}$ .

**Corollary 2.** (Equalized expected set size induces coverage distortion) Suppose Assumption 3 holds. Let the group-wise thresholds  $\{\tau_g\}_{g \in G}$  satisfy  $\ell_g(\tau_g) = \lambda$  for all  $g \in G$ , so that they enforce equalized expected set size at a common level  $\lambda$ . Then the RMS coverage distortion relative to the exact group-wise coverage satisfies

$$\sqrt{\mathbb{E}[(F_{S|G}(\tau_G) - F_{S|G}(q_G))^2]} \geq \kappa_{\text{eff}}(\lambda) \sigma_\lambda. \quad (21)$$

**Take-away.** Equalizing expected set size generally incurs a measurable coverage cost.

Corollary 2 provides the corresponding quantitative statement for the reverse conversion compared to Corollary 1. The induced coverage distortion under equalized size calibration is governed by the dispersion of the coverage-calibrated set sizes and the local coverage-size sensitivity.

Taken together, Corollaries 1 and 2 quantify the cost of the two fairness policies studied in Section 4.1. Corollary 1 measures how intrinsic heterogeneity reappears as set size distortion when exact group-wise coverage is enforced, while Corollary 2 measures how it reappears as coverage distortion when expected set size is equalized across groups.

## 5 Experiments

The results in Sections 3 and 4 were derived using population analysis. Our experiments in this section are not designed as a benchmark comparison against fairness-aware conformal methods;

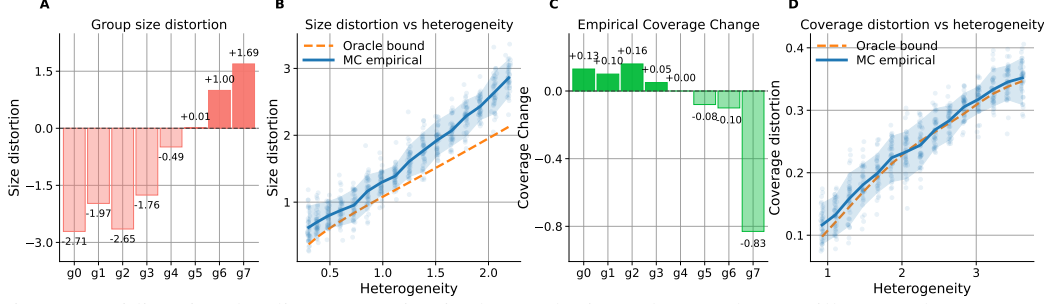


Figure 1: Bidirectional policy conversion in the synthetic study. Panels A–B illustrate the coverage-to-size direction in Theorem 3 and Corollary 1. Panel A shows the signed change in expected set size for each of eight equally weighted groups, and Panel B shows that the aggregate size distortion grows with cross-group score heterogeneity and tracks the oracle lower-bound scale. Panels C–D correspond to the size-to-coverage direction in Theorem 4 and Corollary 2. Panel C reports the signed finite-sample change  $\hat{F}_{S|g}(\hat{\tau}_g) - \hat{F}_{S|g}(\hat{q}_g)$  after replacing empirical group-wise thresholds by equalized-size thresholds; hence the displayed values are changes relative to the empirical group-wise benchmark. Panel D shows that the aggregate coverage distortion grows with heterogeneity.

rather, they are designed to test whether the distortion transfer pattern remains visible under finite-sample calibration, matching how CP is used in practice. We focus on three finite-sample consequences of Sections 3 and 4: the pooled threshold lower-bound behavior (Theorem 2) with the effective lower-bound scale  $m_{\text{eff}}(q)\sigma_{\Delta}$ , the RMS set-size distortion after switching from  $q$  to  $q_g$  (Corollary 1), and the RMS coverage distortion under equalized expected set size (Corollary 2). Our code is available at <https://github.com/GreenPenguin001/group-cp-tradeoffs>.

## 5.1 Synthetic Simulations

We generate calibration and test nonconformity scores directly from known group-conditional score distributions, and then apply the same empirical quantile rule used throughout the paper. This lets us compare finite-sample distortions with the corresponding population lower-bound scales from Sections 3 and 4. Figure 1 studies the bidirectional policy conversion with eight equally weighted groups  $g_0, \dots, g_7$ , and with Gaussian mixture scores for the coverage-to-size direction, and Student- $t$ /Gaussian mixture scores for size-to-coverage. For the policy conversion panels, we use monotone proxy size curves  $\ell_g(t) = a_g + b_g t$  to map thresholds to expected set sizes. In Figure 1, Panels A–B show the coverage-to-size direction in Corollary 1, with oracle scale  $v_{\text{eff}}(q)\sigma_{\Delta}$ ; Panels C–D show the size-to-coverage direction in Corollary 2, with oracle scale  $\kappa_{\text{eff}}(\lambda)\sigma_{\lambda}$ , where coverage change is measured using the empirical quantile  $\hat{q}_g$ . We find that mean distortions in the finite sample case are still bounded by the population analysis results.

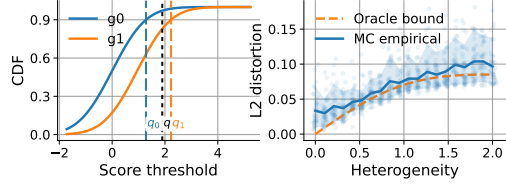


Figure 2: Two-group Gaussian pooled-threshold picture with  $q$  lying between  $q_0$  and  $q_1$ ; across the heterogeneity sweep, the empirical RMS miscoverage remains above the effective lower-bound scale, consistent with Theorem 2.

Figure 2 gives a two-group Gaussian example. To achieve group-wise conditional coverage, one group requires a smaller quantile  $q_0$ , whereas the other requires a larger quantile  $q_1$ . The two groups have different target thresholds, and the pooled threshold lies between them, so under pooled calibration one group is over-covered and the other is under-covered (Theorem 1). As the separation between  $q_0$  and  $q_1$  increases (increasing intrinsic heterogeneity  $\sigma_{\Delta}$ ), the finite-sample mean distortion remains above the oracle effective lower bound (Equation (12)). Together, the synthetic studies support the bidirectional trade-off. All empirical curves use calibration thresholds constructed at target level  $\alpha = 0.1$ , and the reported distortions are evaluated on independent test samples and averaged over 40 Monte Carlo seeds with equal group weights. Detailed score families, heterogeneity ranges, additional diagnostics, and empirical–oracle ratio results under imbalance are deferred to Appendix C.

## 5.2 Bias in Bios Experiments

We use Bias in Bios [6] as a real-data illustration of the policy-conversion mechanism from Sections 3 and 4. We restrict to the ten most frequent professions, two demographic groups (Male

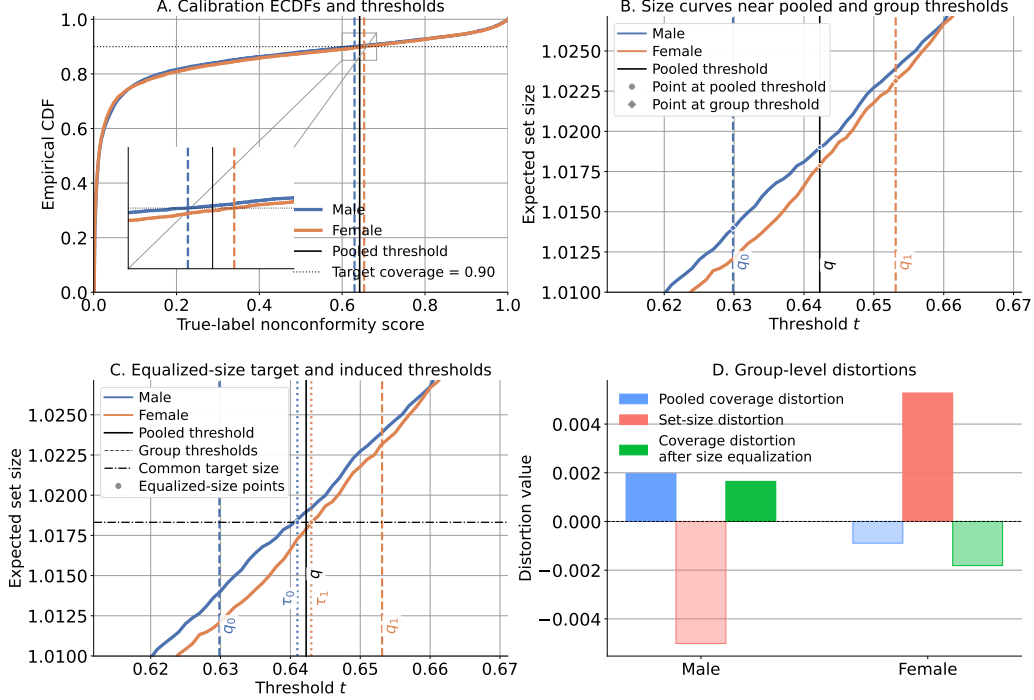


Figure 3: Bias in Bios mechanism view at  $\alpha = 0.1$  for the simple score. Panel A illustrates the pooled-threshold mechanism in Theorem 1; Panels B–C illustrate Theorems 3–4 and Corollaries 1–2; Panel D summarizes the three distortions (Theorem 2, Corollaries 1–2) for male and female groups.

and Female), and use a DistilBERT classifier [21]. Unless otherwise noted, we use the simple nonconformity score  $s(x, y) = 1 - \hat{p}_y(x)$ . In Figure 3, Panel A shows empirical score CDFs with the pooled and distinct group-specific thresholds. Panel B shows that equalizing coverage by moving from  $q$  to  $q_g$  enlarges the cross-group size disparity. Panel C shows the reverse move: equalizing set size requires shifting the thresholds away from  $q_g$ , reintroducing coverage distortion. Panel D summarizes the three distortions. At  $\alpha = 0.1$ , the corresponding RMS quantities, associated with Equations (12), (19) and (21) are 0.0015, 0.0051, and 0.0017, respectively. Thus, Bias in Bios supports the pooled-threshold distortion mechanism in Theorem 2 and the two policy-conversion effects quantified in Corollaries 1 and 2. Detailed per-group quantities are deferred to Table 8. Additional robustness experiments, including alternative score comparisons and finite-calibration diagnostics, are reported in Appendix D.

### 5.3 MultiNLI Experiments

Using the same post-hoc protocol as in Section 5.2, we treat the ten MultiNLI [29] genres as groups. Figure 4 shows the same qualitative transfer pattern (Theorems 3 and 4) for both the simple score,  $s(x, y) = 1 - \hat{p}_y(x)$ , and the RAPS nonconformity score [1]. For the simple score at  $\alpha = 0.1$ , the pooled RMS genre-wise coverage distortion is 0.0150. The corresponding RMS set-size distortion after moving from  $q$  to  $q_g$  is 0.0532. In addition, the RMS coverage distortion under equalized expected set size is 0.0209. Thus, MultiNLI exhibits the signed genre-wise pattern and is consistent with the bidirectional trade-off described in Sections 3 and 4. Per-genre summaries, additional robustness experiments, alternative-score results, and finite-calibration diagnostics are reported in Appendix E.

### 5.4 FACET Experiments

We next show the same mechanisms on FACET [13] using the RAPS score on the age group split (Younger, Middle, Older, Unknown) with a zero-shot CLIP ViT-L/14 classifier [19]. Figure 5 shows the same transfer pattern on a more group imbalanced computer-vision dataset: under pooled calibration, the Younger group is over-covered while the others are under-covered. Switching from  $q$  to  $q_g$  removes the pooled-regime distortion but induces set-size distortion. Equalizing expected set size then reintroduces coverage distortion. Specifically, Panel A shows pooled-threshold coverage distortion, Panel B the set-size shift after equalized coverage, and Panel C the coverage shift after equalized expected size. At  $\alpha = 0.1$ , the empirical pooled RMS coverage distortion is 0.0083.

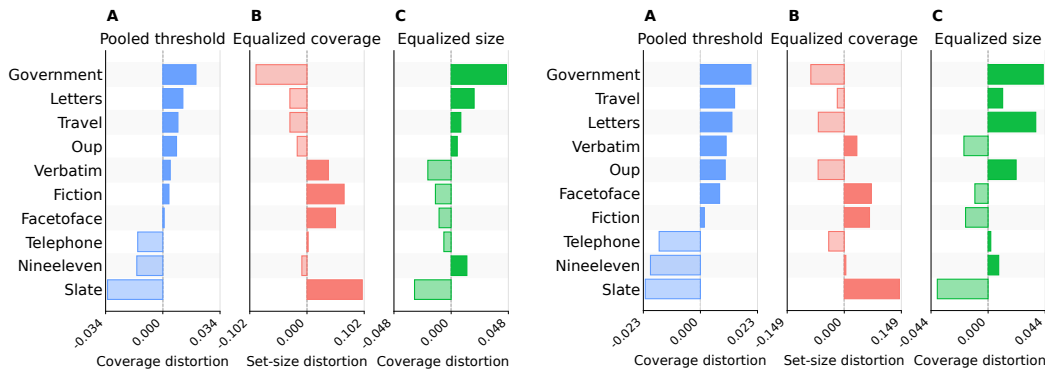


Figure 4: MultiNLI at  $\alpha = 0.1$  with simple (left) and RAPS (right) scores. For each score, Panel A shows signed coverage distortion  $\hat{F}_{S|g}(\hat{q}) - (1 - \alpha)$  under pooled threshold (Theorem 1): positive bars indicate over-coverage and negative bars indicate under-coverage. Panel B shows the signed change in expected set size  $\hat{\ell}_g(\hat{q}_g) - \hat{\ell}_g(\hat{q})$  after switching to group-wise thresholds that equalize coverage (Corollary 1). Panel C shows the signed coverage distortion  $\hat{F}_{S|g}(\hat{\tau}_g) - \hat{F}_{S|g}(\hat{q}_g)$  after enforcing a common expected set size (Corollary 2).

The RMS set-size distortion after changing from  $q$  to  $q_g$  is 0.1717. The RMS coverage distortion under equalized expected set size is 0.0199. Thus, FACET supports the behavior in Theorem 1 together with the two policy-conversion effects quantified in Corollaries 1 and 2. Per-group summaries, additional robustness experiments, and calibration-resampling stability results are reported in Appendix F.

Taken together, the experiments in this section examine three finite-sample consequences of Sections 3 and 4: the pooled-threshold effective lower-bound behavior, the RMS set-size distortion after switching from  $q$  to  $q_g$ , and the RMS coverage distortion under equalized expected set size. We use the effective constants only as oracle/proxy diagnostic scales, not as finite-sample estimators for deployment. Appendix A.5 describes the empirical plug-in diagnostics used to compute the heterogeneity scales and lower-bound proxies reported in our experiments. Additional detectability experiments on how large calibration splits should be for the structural floor to become empirically resolvable are deferred to Appendices D.5, E.5, and F.3.

## 6 Conclusion

We studied group-conditional conformal prediction through the population score distributions underlying split conformal calibration. Our main result is structural: when group-wise conformal quantiles differ, the two group-level objectives studied here, exact group-wise coverage and equalized expected set size, cannot in general be achieved simultaneously. Under a pooled threshold, this heterogeneity appears as a group-wise coverage disparity; enforcing exact group-wise coverage shifts the heterogeneity to expected set size disparity, while equalizing expected set size reintroduces coverage disparity. These results show that the two leading fairness notions in CP, Equalized Coverage and Equalized Set Size, exhibit a structural trade-off, thereby identifying the CP counterpart of classical impossibility results in algorithmic fairness.

Our goal is not to solve full conditional coverage, nor to prescribe a normative fairness criterion. Rather, we identify a population-level constraint induced by heterogeneous group quantiles under conformal calibration. The quantitative bounds rely on local regularity assumptions, including continuity of score distributions and nondegenerate local sensitivity of the set size curves. In addition, the analysis is developed at the level of prespecified discrete groups and population score distributions, while finite-sample behavior is studied empirically. These limitations are deliberate: they separate the structural effect of heterogeneity from broader questions about adaptive subgroup validity, end-to-end training, or fully conditional guarantees.

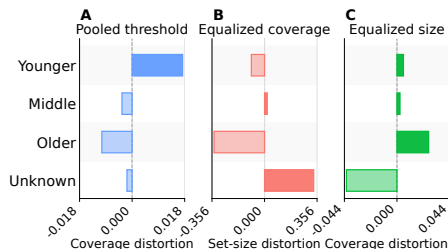


Figure 5: FACET at  $\alpha = 0.1$  with the RAPS score; Panel A illustrates Theorem 1, and Panels B–C illustrate Corollaries 1–2.

In this sense, a calibration policy should be understood not as removing group heterogeneity, but as determining whether it manifests as cross-group disparity in coverage or set size, and how large the resulting policy-conversion distortions will be. A natural next step is to extend the analysis beyond prespecified discrete groups and population score distributions, and to develop finite-sample theory for the policy-conversion distortions. Another is to connect these structural trade-offs to adaptive subgroup validity and to learned calibration policies in practice.

## References

- [1] Anastasios Nikolas Angelopoulos, Stephen Bates, Michael Jordan, and Jitendra Malik. Uncertainty sets for image classifiers using conformal prediction. In *International Conference on Learning Representations*, 2021.
- [2] Francis Bach. A Convex Loss Function for Set Prediction with Optimal Trade-offs Between Size and Conditional Coverage. *arXiv:2512.19142*, 2025.
- [3] Alexandra Chouldechova. Fair prediction with disparate impact: A study of bias in recidivism prediction instruments. *Big data*, 5(2):153–163, 2017. doi: 10.1089/big.2016.0047.
- [4] Jesse C. Cresswell, Yi Sui, Bhargava Kumar, and Noël Vouitsis. Conformal prediction sets improve human decision making. In *Proceedings of the 41st International Conference on Machine Learning*, 2024.
- [5] Jesse C. Cresswell, Bhargava Kumar, Yi Sui, and Mouloud Belbahri. Conformal prediction sets can cause disparate impact. In *The Thirteenth International Conference on Learning Representations*, 2025.
- [6] Maria De-Arteaga, Alexey Romanov, Hanna Wallach, Jennifer Chayes, Christian Borgs, Alexandra Chouldechova, Sahin Geyik, Krishnaram Kenthapadi, and Adam Tauman Kalai. Bias in Bios: A Case Study of Semantic Representation Bias in a High-Stakes Setting. In *Proceedings of the Conference on Fairness, Accountability, and Transparency*, page 120–128, 2019. ISBN 9781450361255. doi: 10.1145/3287560.3287572.
- [7] Aryeh Dvoretzky, Jack Kiefer, and Jacob Wolfowitz. Asymptotic minimax character of the sample distribution function and of the classical multinomial estimator. *The Annals of Mathematical Statistics*, pages 642–669, 1956.
- [8] Rina Foygel Barber, Emmanuel J Candès, Aaditya Ramdas, and Ryan J Tibshirani. The limits of distribution-free conditional predictive inference. *Information and Inference: A Journal of the IMA*, 10(2):455–482, 2021.
- [9] Rina Foygel Barber, Emmanuel J Candès, Aaditya Ramdas, and Ryan J Tibshirani. De finetti’s theorem and related results for infinite weighted exchangeable sequences. *Bernoulli*, 30(4): 3004–3028, 2024.
- [10] Chao Gao, Liren Shan, Vaidehi Srinivas, and Aravindan Vijayaraghavan. Volume optimality in conformal prediction with structured prediction sets. In *Proceedings of the 42nd International Conference on Machine Learning*, volume 267, pages 18495–18527, 2025.
- [11] Isaac Gibbs, John J Cherian, and Emmanuel J Candès. Conformal prediction with conditional guarantees. *Journal of the Royal Statistical Society Series B: Statistical Methodology*, 87(4): 1100–1126, 03 2025. ISSN 1369-7412. doi: 10.1093/jrssb/qkaf008.
- [12] Ozgur Guldogan, Neeraj Sarna, Yuanyuan Li, and Michael Berger. Counterfactually fair conformal prediction. In *Proceedings of The 29th International Conference on Artificial Intelligence and Statistics*, 2026.
- [13] Laura Gustafson, Chloe Rolland, Nikhila Ravi, Quentin Duval, Aaron Adcock, Cheng-Yang Fu, Melissa Hall, and Candace Ross. FACET: Fairness in computer vision evaluation benchmark. In *Proceedings of the IEEE/CVF International Conference on Computer Vision*, pages 20370–20382, 2023.
- [14] Moritz Hardt, Eric Price, and Nati Srebro. Equality of opportunity in supervised learning. In *Advances in Neural Information Processing Systems 29*, pages 3315–3323, 2016.
- [15] Jon Kleinberg, Sendhil Mullainathan, and Manish Raghavan. Inherent trade-offs in the fair determination of risk scores. In *8th Innovations in Theoretical Computer Science Conference*, volume 67, pages 43:1–43:23, 2017. doi: 10.4230/LIPIcs.ITCS.2017.43.
- [16] Claire Lazar Reich and Suhas Vijaykumar. A Possibility in Algorithmic Fairness: Can Calibration and Equal Error Rates Be Reconciled? In *2nd Symposium on Foundations of Responsible Computing*, volume 192, pages 4:1–4:21, 2021. doi: 10.4230/LIPIcs.FORC.2021.4.

- [17] Meichen Liu, Lei Ding, Dengdeng Yu, Wulong Liu, Linglong Kong, and Bei Jiang. Conformalized fairness via quantile regression. *Advances in Neural Information Processing Systems*, 35: 11561–11572, 2022.
- [18] Pengqi Liu, Zijun Yu, Mouloud Belbahri, Arthur Charpentier, Masoud Asgharian, and Jesse C. Cresswell. Beyond procedure: Substantive fairness in conformal prediction. In *Proceedings of the 43rd International Conference on Machine Learning*, 2026. To appear.
- [19] Alec Radford, Jong Wook Kim, Chris Hallacy, Aditya Ramesh, Gabriel Goh, Sandhini Agarwal, Girish Sastry, Amanda Askell, Pamela Mishkin, Jack Clark, Gretchen Krueger, and Ilya Sutskever. Learning Transferable Visual Models From Natural Language Supervision. In *Proceedings of the 38th International Conference on Machine Learning*, volume 139, pages 8748–8763, 2021.
- [20] Yaniv Romano, Rina Foygel Barber, Chiara Sabatti, and Emmanuel Candès. With malice toward none: Assessing uncertainty via equalized coverage. *Harvard Data Science Review*, 2(2):4, 2020.
- [21] Victor Sanh, Lysandre Debut, Julien Chaumond, and Thomas Wolf. DistilBERT, a distilled version of BERT: smaller, faster, cheaper and lighter. *arXiv:1910.01108*, 2019.
- [22] Glenn Shafer and Vladimir Vovk. A Tutorial on Conformal Prediction. *Journal of Machine Learning Research*, 9(12):371–421, 2008.
- [23] Bernard W Silverman. *Density estimation for statistics and data analysis*. Routledge, 2018.
- [24] Davut Emre Tasar. The coverage-deferral trade-off: Fairness implications of conformal prediction in human-in-the-loop decision systems. *Preprints*, 2025. doi: 10.20944/preprints202512.2631.v1.
- [25] Aditya T. Vadlamani, Anutam Srinivasan, Pranav Maneriker, Ali Payani, and Srinivasan Parthasarathy. A generic framework for conformal fairness. In *The Thirteenth International Conference on Learning Representations*, 2025.
- [26] Vladimir Vovk, David Lindsay, Ilia Nouretdinov, and Alex Gammerman. Mondrian confidence machine. *Technical Report*, 2003.
- [27] Vladimir Vovk, Alexander Gammerman, and Glenn Shafer. *Algorithmic learning in a random world*. Springer, 2005.
- [28] Fangxin Wang, Lu Cheng, Ruocheng Guo, Kay Liu, and Philip S Yu. Equal opportunity of coverage in fair regression. *Advances in Neural Information Processing Systems*, 36:7743–7755, 2023.
- [29] Adina Williams, Nikita Nangia, and Samuel Bowman. A broad-coverage challenge corpus for sentence understanding through inference. In *Proceedings of the 2018 Conference of the North American Chapter of the Association for Computational Linguistics: Human Language Technologies, Volume 1 (Long Papers)*, pages 1112–1122, 2018. doi: 10.18653/v1/N18-1101.
- [30] Yanfei Zhou and Matteo Sesia. Conformal classification with equalized coverage for adaptively selected groups. *Advances in Neural Information Processing Systems*, 37:108760–108823, 2024.

## Appendix Contents

- [Appendix A: Technical Discussion](#)
- [Appendix B: Proofs of Theoretical Results](#)
- [Appendix C: Additional Experimental Details](#)
- [Appendix D: Bias in Bios Experiments](#)
- [Appendix E: MultiNLI Experiments](#)
- [Appendix F: FACET Experiments](#)
- [Appendix G: Computational Resources](#)

## A Technical Discussion

### A.1 Two-group Specialization of the Conservation Law and Uncertainty Relations

In finite-sample split conformal prediction, the empirical quantile  $\hat{q}$  satisfies the identity (7) approximately and converges to the population identity asymptotically. We first formalize a two-group version of the conservation law. Let  $K = 2$ , with groups  $g \in \{0, 1\}$  and  $p := \mathbb{P}(G = 1) \in (0, 1)$ . Without loss of generality, we assume the two quantiles satisfy  $q_0 < q_1$ . The distance between them is denoted by  $\Delta := q_1 - q_0$ . For notational convenience, in the two-group case we write  $F_0 := F_{S|0}$  and  $F_1 := F_{S|1}$ . Whenever densities exist, we likewise write  $f_0 := f_{S|0}$  and  $f_1 := f_{S|1}$ .

**Lemma 1.** *Assume  $q_0 < q_1$ ,  $p \in (0, 1)$  and that  $F_0$  and  $F_1$  are continuous. Then the pooled quantile  $q = F_S^{-1}(1 - \alpha)$  satisfies  $q \in [q_0, q_1]$ .*

**Assumption 5** (Local density lower bounds for two-group case). For each group  $g \in \{0, 1\}$ , the conditional distribution of scores admits a density  $f_{S|g}$  on the interval  $[q_0, q_1]$  and  $\text{ess inf}_{t \in [q_0, q_1]} f_0(t) \geq m_0 > 0$ , and  $\text{ess inf}_{t \in [q_0, q_1]} f_1(t) \geq m_1 > 0$ .

We define the over- and under-coverage magnitudes  $\omega_o := \varepsilon_0(q) = F_0(q) - (1 - \alpha)$ ,  $\omega_u := -\varepsilon_1(q) = (1 - \alpha) - F_1(q)$ . By Theorem 1, the two-group conservation identity gives

$$(1 - p)\omega_o = p\omega_u \quad \iff \quad \omega_o = \frac{p}{1 - p}\omega_u. \quad (22)$$

Finally, we write

$$\rho := \frac{p}{1 - p}, \quad B_{01} := \frac{\Delta}{\frac{1}{m_1} + \rho \frac{1}{m_0}}. \quad (23)$$

Next, we present the two-group uncertainty relation in the following theorem.

**Theorem 5.** *(Two-group product-type uncertainty relation) Suppose Assumption 5 holds. Let  $q_0 < q_1$ . Then*

$$\omega_u \geq B_{01}, \quad (24)$$

$$\omega_o \geq \rho B_{01}, \quad (25)$$

$$\omega_u \omega_o \geq \rho B_{01}^2. \quad (26)$$

We note that the constant  $\Delta$  is an intrinsic heterogeneity disparity at level  $1 - \alpha$ . The ratio  $p/(1 - p)$  quantifies how much the pooled threshold is pulled toward group 1. The terms  $m_0$  and  $m_1$  encode local score sensitivities, implying that smaller local densities amplify the threshold displacement required to compensate for a given level of group-wise miscoverage. We next extend this product-type statement to the multi-group setting.

### A.2 Generalization of a Product-type Conservation Law and Uncertainty Relation

The two-group statement above admits the following aggregate multi-group extension.

**Assumption 6** (Local density lower bounds for multi-group case). Let  $q_{\min} := \min_{g \in \mathcal{G}} q_g$  and  $q_{\max} := \max_{g \in \mathcal{G}} q_g$ , with  $q_{\min} < q_{\max}$ , and let  $q \in (q_{\min}, q_{\max})$  be the threshold under consideration. For each group  $g \in \mathcal{G}$ ,  $F_{S|g}$  is absolutely continuous on  $[q_{\min}, q_{\max}]$ , satisfies  $F_{S|g}(q_g) = 1 - \alpha$ , and has density  $f_{S|g}$  satisfying  $f_{S|g}(t) \geq m_g > 0$  for almost every  $t \in [q_{\min}, q_{\max}]$ .

Table 1: Notation summary

Symbol	Meaning
$\mathcal{G} = \{1, \dots, K\}$	Prespecified discrete group set.
$G(X), p_g$	Group label of $X$ and group proportion $p_g = \mathbb{P}(G(X) = g)$ .
$S$	Nonconformity score.
$F_{S g}(t)$	Conditional score CDF for group $g$ : $\mathbb{P}(S \leq t   G = g)$ .
$q_g$	Group-specific $1 - \alpha$ quantile of $F_{S g}$ .
$F_S(t)$	Mixture score CDF: $\sum_{g \in \mathcal{G}} p_g F_{S g}(t)$ .
$q$	Pooled $1 - \alpha$ quantile of $F_S$ .
$\varepsilon_g(q)$	Group-wise miscoverage under pooled $q$ : $F_{S g}(q) - (1 - \alpha)$ .
$q_G, \varepsilon_G(q)$	Random-group versions of $q_g$ and $\varepsilon_g(q)$ when $G \sim p$ .
$\sigma_\Delta$	Cross-group quantile heterogeneity: $\text{sd}(q_G)$ .
$\ell_g(t)$	Expected set size for group $g$ at threshold $t$ .
$\lambda_g$	Coverage-calibrated expected set size for group $g$ : $\ell_g(q_g)$ .
$\tau_g$	Group-wise threshold satisfying $\ell_g(\tau_g) = \lambda$ under an equalized size.
$m_g(q), m_{\text{eff}}(q)$	Local score density stiffness and its effective aggregate version.
$v_g, v_{\text{eff}}(q)$	Local responsiveness of $\ell_g$ and its aggregate version.
$\kappa_g, \kappa_{\text{eff}}(\lambda)$	Local coverage–size conversion factor and its aggregate version.
$\sigma_\lambda$	Dispersion of coverage-calibrated set size: $\sigma_\lambda = \text{sd}(\lambda_G)$ .

We define the over- and under-coverage magnitudes for  $K$  groups as

$$\Omega_o(q) := \sum_{\varepsilon_g(q) > 0} p_g \varepsilon_g(q), \quad \Omega_u(q) := \sum_{\varepsilon_g(q) < 0} p_g [-\varepsilon_g(q)], \quad (27)$$

and

$$w_g := p_g m_g, \quad \bar{q}_m := \frac{\sum_{g \in \mathcal{G}} w_g q_g}{\sum_{g \in \mathcal{G}} w_g}, \quad B_K := \frac{1}{2} \sum_{g \in \mathcal{G}} w_g |q_g - \bar{q}_m|. \quad (28)$$

**Theorem 6.** (Generalization of a product-type uncertainty relation)

Suppose Assumption 6 holds. Then

1.  $\max\{\Omega_o(q), \Omega_u(q)\} \geq B_K$  and  $\min\{\Omega_o(q), \Omega_u(q)\} \geq (B_K - |\delta(q)|)_+$ , where  $(x)_+ = \max\{x, 0\}$ .
2.  $\Omega_o(q) \Omega_u(q) \geq B_K (B_K - |\delta(q)|)_+$ .
3. Under exact conservation,  $\delta(q) = 0$ , we have  $\Omega_o(q) \Omega_u(q) \geq B_K^2$ .

When  $q$  is the pooled population quantile and the mixture CDF  $F_S$  is continuous at  $q$ , Theorem 1 gives  $\delta(q) = 0$ , so the exact-conservation form in part 3 is the relevant pooled-calibration case.

Theorem 6 refines Theorem 1 from a signed additive conservation law to a magnitude lower bound. The product-type form echoes the fact that pooled calibration does not remove group heterogeneity but redistributes it into over- and under-coverage aggregates.

### A.3 Coverage Disparity and Quantile Variance

In this section, we give an elaboration of Theorem 2 when  $\mathbb{E}[\varepsilon_G(q)] = 0$ . The resulting inequality exhibits a Cramér–Rao-type structure.

**Definition 2.** For each group, define the segment average density

$$\bar{f}_{S|g}(q) := \begin{cases} \frac{F_{S|g}(q) - F_{S|g}(q_g)}{q - q_g} = \frac{\varepsilon_g(q)}{q - q_g}, & q \neq q_g, \\ 1, & q = q_g. \end{cases} \quad (29)$$

Assume  $\bar{f}_{S|g}(q) > 0$  for all groups with  $q \neq q_g$ ; when  $q = q_g$ , the corresponding term in (30) is zero. We define the apparatus cost term

$$L(q) := \sqrt{\mathbb{E}\left[\left(\frac{q - q_G}{\bar{f}_{S|G}(q)}\right)^2\right]}. \quad (30)$$

**Theorem 7.** *Suppose Assumption 1 holds. With Definition 2,*

$$\sqrt{\mathbb{E}[\varepsilon_G(q)^2]} \cdot L(q) \geq \mathbb{E}[(q - q_G)^2] \geq \sigma_\Delta^2. \quad (31)$$

The term  $L(q)$  measures the inevitable cost of imposing a pooled  $q$ . The term is large for groups whose quantile displacement is large relative to the induced coverage distortion. In particular, the term quantifies how much the device must move to compensate for heterogeneity. The inequality (31) states that one cannot simultaneously make RMS miscoverage small and keep the apparatus cost small when  $\sigma_\Delta$  is non-negligible.

The Cauchy–Schwarz step in Theorem 7 also has a Hölder version. Let  $r, s \in [1, \infty]$  be conjugate exponents,  $1/r + 1/s = 1$ . Under Definition 2,

$$\|\varepsilon_G(q)\|_{L^r(p)} \left\| \frac{q - q_G}{\bar{f}_{S|G}(q)} \right\|_{L^s(p)} \geq \mathbb{E}[(q - q_G)^2] \geq \sigma_\Delta^2. \quad (32)$$

Indeed, writing  $Q = q - q_G$ , Definition 2 gives  $|\varepsilon_G(q)| = \bar{f}_{S|G}(q)|Q|$ , and hence

$$\mathbb{E}[Q^2] = \mathbb{E} \left[ |\varepsilon_G(q)| \left| \frac{Q}{\bar{f}_{S|G}(q)} \right| \right]. \quad (33)$$

Applying Hölder’s inequality gives the first inequality. The second follows from

$$\mathbb{E}[(q - q_G)^2] \geq \text{Var}(q_G) = \sigma_\Delta^2. \quad (34)$$

Taking  $r = s = 2$  recovers Theorem 7.

#### A.4 Connection to Classical Fairness Impossibility Results

A closely related precursor appears in the algorithmic fairness literature. Specifically, Chouldechova [3] shows that in binary settings, when two groups have different base rates,  $\pi_g = \mathbb{P}(Y = 1 | G = g)$ , predictive parity, i.e., equal PPV $_g = \mathbb{P}(Y = 1 | \hat{Y} = 1, G = g)$  across groups, cannot generally hold simultaneously with equalized error profiles matching the false positive rates  $\text{FPR}_g = \mathbb{P}(\hat{Y} = 1 | Y = 0, G = g)$  and the true positive rates  $\text{TPR}_g = \mathbb{P}(\hat{Y} = 1 | Y = 1, G = g)$ . The incompatibility follows from a Bayes coupling identity relating predictive values, base rates, and the likelihood ratio  $\text{TPR}_g/\text{FPR}_g$ . Expressed in log-odds form, one may rewrite the incompatibility in the following multiplicative form

$$\exp(|\Delta \logit(\text{PPV})|) \exp(|\Delta \log(\text{TPR}/\text{FPR})|) \geq \exp(|\Delta \logit(\pi)|), \quad (35)$$

where  $\logit(x) = \log(x/(1-x))$  and  $\Delta f := f_1 - f_2$ . The two exponential terms quantify deviations from predictive parity and from equalized error rate structure, while the right-hand side depends only on the base rate gap. Thus, in that setting, unequal base rates act as a structural lower bound that prevents fairness deviations from simultaneously vanishing.

#### A.5 Practical Plug-in Diagnostics

Our experiments use empirical plug-in diagnostics for the heterogeneity scales and effective lower-bound proxies. For these diagnostics,  $\hat{q}$  and  $\hat{q}_g$  are computed from the calibration split, whereas  $\hat{p}_g$ ,  $\hat{F}_{S|g}$ ,  $\hat{\ell}_g$ , and the reported RMS distortions are computed on the corresponding test sample, namely the independent test sample in the synthetic simulations and the test split in the real-data experiments. The quantile heterogeneity can be estimated by

$$\hat{\sigma}_\Delta^2 = \sum_g \hat{p}_g \left( \hat{q}_g - \sum_h \hat{p}_h \hat{q}_h \right)^2.$$

For any threshold  $t$ , let

$$\hat{F}_{S|g}(t) = \frac{1}{n_g} \sum_{i:G_i=g} \mathbf{1}\{S_i \leq t\}, \quad \hat{\ell}_g(t) = \frac{1}{n_g} \sum_{i:G_i=g} |\hat{C}_t(X_i)|$$

be the empirical group score CDF and empirical set-size curve on this test sample, where  $n_g$  is the number of test examples in group  $g$ . Rather than estimating essential infima, segment-average proxies along the same policy-conversion paths are:

$$\hat{m}_g^{\text{seg}} = \frac{|\hat{F}_{S|g}(\hat{q}) - \hat{F}_{S|g}(\hat{q}_g)|}{|\hat{q} - \hat{q}_g|}, \quad \hat{v}_g^{\text{seg}} = \frac{|\hat{\ell}_g(\hat{q}_g) - \hat{\ell}_g(\hat{q})|}{|\hat{q}_g - \hat{q}|}.$$

Next, define

$$\hat{\lambda}_g := \hat{\ell}_g(\hat{q}_g), \quad \hat{\lambda} := \sum_g \hat{p}_g \hat{\lambda}_g, \quad \hat{\sigma}_\lambda^2 = \sum_g \hat{p}_g (\hat{\lambda}_g - \hat{\lambda})^2.$$

If  $\hat{\tau}_g$  is the empirical threshold used to attain the common size target  $\hat{\lambda}$ , then

$$\hat{\kappa}_g^{\text{seg}} = \frac{|\hat{F}_{S|g}(\hat{\tau}_g) - \hat{F}_{S|g}(\hat{q}_g)|}{|\hat{\lambda} - \hat{\lambda}_g|}.$$

When a denominator is zero, the corresponding segment proxy is set to zero.

Finally, for group-wise coefficients  $a_g$  and gaps  $d_g$ , define

$$\mathcal{E}(a, d) = \left( \frac{\sum_g \hat{p}_g a_g^2 d_g^2}{\sum_g \hat{p}_g d_g^2} \right)^{1/2},$$

which can be used to compute

$$\hat{m}_{\text{eff}}^{\text{seg}} = \mathcal{E}(\hat{m}^{\text{seg}}, \hat{q} - \hat{q}_g), \quad \hat{v}_{\text{eff}}^{\text{seg}} = \mathcal{E}(\hat{v}^{\text{seg}}, \hat{q} - \hat{q}_g), \quad \hat{\kappa}_{\text{eff}}^{\text{seg}} = \mathcal{E}(\hat{\kappa}^{\text{seg}}, \hat{\lambda}_g - \hat{\lambda}),$$

yielding the diagnostic scales

$$\hat{m}_{\text{eff}}^{\text{seg}} \hat{\sigma}_\Delta, \quad \hat{v}_{\text{eff}}^{\text{seg}} \hat{\sigma}_\Delta, \quad \hat{\kappa}_{\text{eff}}^{\text{seg}} \hat{\sigma}_\lambda.$$

These quantities are empirical diagnostic proxy scales for assessing whether group heterogeneity is large enough for coverage or set-size distortions to be visible.

## B Proofs of Theoretical Results

### Proof of Theorem 1

**Theorem 1.** (Conservation law for pooled calibration) Let  $p_g := \mathbb{P}\{G(X) = g\}$  be the group mass. Group-wise coverage distortion  $\varepsilon_g(q)$  under the pooled threshold satisfies the aggregate identity

$$\sum_{g \in \mathcal{G}} p_g \varepsilon_g(q) = F_S(q) - (1 - \alpha) =: \delta(q). \quad (7)$$

If  $F_S$  is continuous at  $q$ , then  $\delta(q) = 0$ , and hence  $\sum_{g \in \mathcal{G}} p_g \varepsilon_g(q) = 0$ .

*Proof.* By definition of  $F_S$ ,

$$\sum_{g \in \mathcal{G}} p_g \varepsilon_g(q) = \sum_{g \in \mathcal{G}} p_g F_{S|g}(q) - (1 - \alpha) = F_S(q) - (1 - \alpha) = \delta(q) \geq 0,$$

which yields the generalized conservation law. If  $F_S$  is continuous at  $q$ , then by definition of the quantile  $F_S(t) < 1 - \alpha$  for all  $t < q$ ; hence, we have  $F_S(q^-) \leq 1 - \alpha$ . The continuity at  $q$  gives

$$F_S(q) = F_S(q^-) \leq 1 - \alpha,$$

while definition of  $q$  gives  $F_S(q) \geq 1 - \alpha$ . Thus, we have  $F_S(q) = 1 - \alpha$ , i.e.,  $\delta(q) = 0$ . □

## Proof of Theorem 2

**Theorem 2.** (Pooled-threshold uncertainty relation) Suppose Assumption 1 holds. Then

$$\text{Var}(\varepsilon_G(q)) \geq m_{\text{eff}}(q)^2 \text{Var}(q_G). \quad (12)$$

*Proof.* If  $\mathbb{E}[(q - q_G)^2] = 0$ , then  $\text{Var}(q_G) = 0$ , so the claim is trivial. We therefore assume  $\mathbb{E}[(q - q_G)^2] > 0$ , so that  $m_{\text{eff}}(q)$  is well defined.

Fix a group  $g \in \mathcal{G}$ . Since  $q_g$  is the group-specific  $1 - \alpha$  quantile and  $F_{S|g}$  is continuous on the relevant segment,  $F_{S|g}(q_g) = 1 - \alpha$ . Hence, by Assumption 1,

$$\varepsilon_g(q) = F_{S|g}(q) - F_{S|g}(q_g) = \int_{q_g}^q f_{S|g}(t) dt.$$

By the definition of  $m_g(q)$ ,

$$|\varepsilon_g(q)| = \left| \int_{q_g}^q f_{S|g}(t) dt \right| \geq m_g(q) |q - q_g|.$$

Squaring and averaging over  $G \sim p$  gives

$$\mathbb{E}[\varepsilon_G(q)^2] \geq \mathbb{E}[m_G(q)^2 (q - q_G)^2].$$

By the definition of  $m_{\text{eff}}(q)$ ,

$$\mathbb{E}[m_G(q)^2 (q - q_G)^2] = m_{\text{eff}}(q)^2 \mathbb{E}[(q - q_G)^2].$$

Moreover,

$$\mathbb{E}[(q - q_G)^2] = \text{Var}(q_G) + (q - \mathbb{E}[q_G])^2 \geq \text{Var}(q_G).$$

Finally, Assumption 1 implies that the mixture CDF  $F_S$  is continuous at  $q$ , so Theorem 1 gives

$$\mathbb{E}[\varepsilon_G(q)] = \sum_{g \in \mathcal{G}} p_g \varepsilon_g(q) = 0.$$

Therefore,

$$\text{Var}(\varepsilon_G(q)) = \mathbb{E}[\varepsilon_G(q)^2] \geq m_{\text{eff}}(q)^2 \text{Var}(q_G).$$

□

## Proof of Theorem 3

**Theorem 3.** (Equalized coverage induces cross-group expected set size disparity) Assume the score CDF  $F_{S|g}$  is continuous and the map  $t \mapsto \ell_g(t)$  is non-decreasing for all  $g \in \mathcal{G}$ . Suppose Assumption 2 holds for some reference group  $r \in \mathcal{G}$ . Then,

1. The group-wise thresholds  $\{q_g\}_{g \in \mathcal{G}}$ , which achieve an exact group-wise coverage level  $1 - \alpha$ , necessarily induce a nonzero cross-group disparity in expected set size. More precisely, for every  $g \in \mathcal{H}_r \setminus \{r\}$ ,  $\ell_g(q_g) - \ell_r(q_r) \geq c_g > 0$ .

Consequently,

$$\max_{g, g' \in \mathcal{G}} |\ell_g(q_g) - \ell_{g'}(q_{g'})| \geq \max_{g \in \mathcal{H}_r \setminus \{r\}} c_g > 0. \quad (14)$$

Therefore, exact group-wise coverage cannot simultaneously satisfy equalized expected set size across groups.

2. The restricted mean squared cross-group size disparity relative to the reference group  $r$  satisfies

$$D_r^2 = \sum_{g \in \mathcal{H}_r \setminus \{r\}} p_g (\ell_g(q_g) - \ell_r(q_r))^2 \geq \sum_{g \in \mathcal{H}_r \setminus \{r\}} p_g c_g^2 > 0. \quad (15)$$

*Proof.* The group-wise thresholds  $\{q_g\}_{g \in \mathcal{G}}$  achieve equalized coverage at level  $1 - \alpha$  across groups. Now fix any  $g \in \mathcal{H}_r \setminus \{r\}$ . By definition of  $\mathcal{H}_r$ , we have  $q_g \geq q_r$ . Since  $t \mapsto \ell_g(t)$  is non-decreasing,

$$\ell_g(q_g) \geq \ell_g(q_r).$$

Subtracting  $\ell_r(q_r)$  from both sides and using Assumption 2 gives

$$\ell_g(q_g) - \ell_r(q_r) \geq \ell_g(q_r) - \ell_r(q_r) \geq c_g > 0.$$

This proves the first displayed claim.

Taking the maximum over  $g \in \mathcal{H}_r \setminus \{r\}$  yields

$$\max_{g, g' \in \mathcal{G}} |\ell_g(q_g) - \ell_{g'}(q_{g'})| \geq \max_{g \in \mathcal{H}_r \setminus \{r\}} |\ell_g(q_g) - \ell_r(q_r)| \geq \max_{g \in \mathcal{H}_r \setminus \{r\}} c_g > 0.$$

Thus, equalized expected set size across all groups is impossible under the equalized group-wise coverage policy.

For the mean square claim, using the previously established bound for each  $g \in \mathcal{H}_r \setminus \{r\}$ ,

$$(\ell_g(q_g) - \ell_r(q_r))^2 \geq c_g^2.$$

Multiplying by  $p_g$  and summing over  $g \in \mathcal{H}_r \setminus \{r\}$  gives

$$D_r^2 = \sum_{g \in \mathcal{H}_r \setminus \{r\}} p_g (\ell_g(q_g) - \ell_r(q_r))^2 \geq \sum_{g \in \mathcal{H}_r \setminus \{r\}} p_g c_g^2 > 0.$$

This proves the claim.  $\square$

#### Proof of Theorem 4

**Theorem 4.** (Equalized expected set size induces cross-group coverage disparity) Suppose Assumption 3 holds, and suppose for some common target level  $\lambda$  the thresholds  $\{\tau_g\}_{g \in \mathcal{G}}$  satisfy  $\ell_g(\tau_g) = \lambda$ ,  $g \in \mathcal{G}$ . Then the following results hold.

(i) For every group  $g$  with  $\lambda_g < \lambda$ ,  $F_{S|g}(\tau_g) - (1 - \alpha) \geq \kappa_g (\lambda - \lambda_g)$ .

(ii) For every group  $g'$  with  $\lambda_{g'} > \lambda$ ,  $(1 - \alpha) - F_{S|g'}(\tau_{g'}) \geq \kappa_{g'} (\lambda_{g'} - \lambda)$ .

Consequently, for any pair  $g, g' \in \mathcal{G}$  such that  $\lambda_g < \lambda < \lambda_{g'}$ , we have the pairwise lower bound

$$F_{S|g}(\tau_g) - F_{S|g'}(\tau_{g'}) \geq \kappa_g (\lambda - \lambda_g) + \kappa_{g'} (\lambda_{g'} - \lambda). \quad (16)$$

In particular, if there exist groups  $g, g'$  with  $\lambda_g < \lambda_{g'}$  and  $\lambda \in (\lambda_g, \lambda_{g'})$ , then

$$\max_{a, b \in \mathcal{G}} |F_{S|a}(\tau_a) - F_{S|b}(\tau_b)| \geq \kappa_g (\lambda - \lambda_g) + \kappa_{g'} (\lambda_{g'} - \lambda) > 0. \quad (17)$$

*Proof.* Fix a group  $g \in \mathcal{G}$ . If  $\lambda_g < \lambda$ , then, since  $\ell_g$  is monotone on the segment between  $q_g$  and  $\tau_g$  and  $\ell_g(q_g) = \lambda_g$ , the identity  $\ell_g(\tau_g) = \lambda$  implies

$$\tau_g > q_g.$$

By absolute continuity and Assumption 3,

$$\lambda - \lambda_g = \ell_g(\tau_g) - \ell_g(q_g) = \int_{q_g}^{\tau_g} \ell'_g(t) dt.$$

Hence

$$\lambda - \lambda_g \leq \int_{q_g}^{\tau_g} |\ell'_g(t)| dt \leq V_g (\tau_g - q_g),$$

so that

$$\tau_g - q_g \geq \frac{\lambda - \lambda_g}{V_g}.$$

Again by Assumption 3,

$$F_{S|g}(\tau_g) - F_{S|g}(q_g) = \int_{q_g}^{\tau_g} f_{S|g}(t) dt \geq m_g (\tau_g - q_g) \geq \frac{m_g}{V_g} (\lambda - \lambda_g) = \kappa_g (\lambda - \lambda_g).$$

Since  $F_{S|g}(q_g) = 1 - \alpha$ , this proves

$$F_{S|g}(\tau_g) - (1 - \alpha) \geq \kappa_g (\lambda - \lambda_g).$$

Now suppose  $\lambda_{g'} > \lambda$ . Since  $\ell_{g'}(q_{g'}) = \lambda_{g'}$  and  $\ell_{g'}(\tau_{g'}) = \lambda$ , we have

$$\ell_{g'}(q_{g'}) > \ell_{g'}(\tau_{g'}).$$

Because  $\ell_{g'}$  is non-decreasing on the segment between  $q_{g'}$  and  $\tau_{g'}$ , this implies

$$\tau_{g'} < q_{g'}.$$

Indeed, if  $\tau_{g'} \geq q_{g'}$ , monotonicity would imply

$$\ell_{g'}(\tau_{g'}) \geq \ell_{g'}(q_{g'}),$$

contradicting  $\ell_{g'}(\tau_{g'}) < \ell_{g'}(q_{g'})$ . Then

$$\lambda_{g'} - \lambda = \ell_{g'}(q_{g'}) - \ell_{g'}(\tau_{g'}) = \int_{\tau_{g'}}^{q_{g'}} \ell'_{g'}(t) dt \leq \int_{\tau_{g'}}^{q_{g'}} |\ell'_{g'}(t)| dt \leq V_{g'}(q_{g'} - \tau_{g'}),$$

hence

$$q_{g'} - \tau_{g'} \geq \frac{\lambda_{g'} - \lambda}{V_{g'}}.$$

Using Assumption 3 again,

$$F_{S|g'}(q_{g'}) - F_{S|g'}(\tau_{g'}) = \int_{\tau_{g'}}^{q_{g'}} f_{S|g'}(t) dt \geq m_{g'}(q_{g'} - \tau_{g'}) \geq \frac{m_{g'}}{V_{g'}}(\lambda_{g'} - \lambda) = \kappa_{g'}(\lambda_{g'} - \lambda).$$

Since  $F_{S|g'}(q_{g'}) = 1 - \alpha$ , we obtain

$$(1 - \alpha) - F_{S|g'}(\tau_{g'}) \geq \kappa_{g'}(\lambda_{g'} - \lambda).$$

Finally, if  $\lambda_g < \lambda < \lambda_{g'}$ , then combining the two inequalities gives

$$F_{S|g}(\tau_g) - F_{S|g'}(\tau_{g'}) = (F_{S|g}(\tau_g) - (1 - \alpha)) + ((1 - \alpha) - F_{S|g'}(\tau_{g'})) \geq \kappa_g(\lambda - \lambda_g) + \kappa_{g'}(\lambda_{g'} - \lambda).$$

Because  $\lambda_g < \lambda < \lambda_{g'}$ , both terms on the right-hand side are strictly positive, and hence the right-hand side is  $> 0$ . Therefore

$$\max_{a,b \in \mathcal{G}} |F_{S|a}(\tau_a) - F_{S|b}(\tau_b)| \geq F_{S|g}(\tau_g) - F_{S|g'}(\tau_{g'}) > 0,$$

which proves that coverage cannot be equalized across groups under this equalized-size policy.  $\square$

### Proof of Corollary 1

**Corollary 1.** (Exact group-wise coverage induces set size distortion) Suppose Assumption 4 holds. Let the pooled threshold  $q$  be replaced by the group-wise thresholds  $\{q_g\}$ . Then the RMS set size lower bound is

$$\sqrt{\mathbb{E}[(\ell_G(q_G) - \ell_G(q))^2]} \geq v_{\text{eff}}(q) \sigma_{\Delta}. \quad (19)$$

*Proof.* Let  $g$  be fixed. By Assumption 4 and the fundamental theorem of calculus, we have

$$\ell_g(q_g) - \ell_g(q) = \int_q^{q_g} \ell'_g(t) dt.$$

Under Assumption 4,  $|\ell'_g(t)| \geq v_g$  along the segment between  $q$  and  $q_g$ , hence  $|\ell_g(q_g) - \ell_g(q)| \geq v_g|q_g - q|$ . Squaring and averaging gives  $\mathbb{E}[(\ell_G(q_G) - \ell_G(q))^2] \geq \mathbb{E}[v_G^2(q_G - q)^2]$ . Taking square roots and using the definition of  $v_{\text{eff}}(q)$  gives  $\sqrt{\mathbb{E}[(\ell_G(q_G) - \ell_G(q))^2]} \geq v_{\text{eff}}(q) \sqrt{\mathbb{E}[(q_G - q)^2]}$ . Since  $\mathbb{E}[(q_G - q)^2] \geq \text{Var}(q_G) = \sigma_{\Delta}^2$ , the desired bound follows.  $\square$

## Proof of Corollary 2

**Corollary 2.** (Equalized expected set size induces coverage distortion) Suppose Assumption 3 holds. Let the group-wise thresholds  $\{\tau_g\}_{g \in G}$  satisfy  $\ell_g(\tau_g) = \lambda$  for all  $g \in G$ , so that they enforce equalized expected set size at a common level  $\lambda$ . Then the RMS coverage distortion relative to the exact group-wise coverage satisfies

$$\sqrt{\mathbb{E}[(F_{S|G}(\tau_G) - F_{S|G}(q_G))^2]} \geq \kappa_{\text{eff}}(\lambda)\sigma_\lambda. \quad (21)$$

*Proof.* We fix group  $g$ . Since  $\ell_g(q_g) = \lambda_g$  by definition, we have

$$\lambda - \lambda_g = \ell_g(\tau_g) - \ell_g(q_g) = \int_{q_g}^{\tau_g} \ell'_g(t) dt.$$

Therefore,  $|\lambda - \lambda_g| \leq V_g |\tau_g - q_g|$ , which implies

$$|\tau_g - q_g| \geq \frac{|\lambda - \lambda_g|}{V_g}.$$

Moreover,

$$|F_{S|g}(\tau_g) - F_{S|g}(q_g)| = \left| \int_{q_g}^{\tau_g} f_{S|g}(t) dt \right| \geq m_g |\tau_g - q_g| \geq m_g \frac{|\lambda - \lambda_g|}{V_g}.$$

Squaring, averaging, taking square roots, and using the definition of  $\kappa_{\text{eff}}(\lambda)$  gives

$$\sqrt{E[(F_{S|G}(\tau_G) - F_{S|G}(q_G))^2]} \geq \kappa_{\text{eff}}(\lambda) \sqrt{E[(\lambda - \lambda_G)^2]}. \quad (36)$$

Since  $E[(\lambda - \lambda_G)^2] \geq \text{Var}(\lambda_G) = \sigma_\lambda^2$ , the desired bound follows.  $\square$

## Proof of Lemma 1

**Lemma 1.** Assume  $q_0 < q_1$ ,  $p \in (0, 1)$  and that  $F_0$  and  $F_1$  are continuous. Then the pooled quantile  $q = F_S^{-1}(1 - \alpha)$  satisfies  $q \in [q_0, q_1]$ .

*Proof.* Assume  $q < q_0$  and prove by contradiction: Given  $q < q_0$ , we have  $q < q_1$  since  $q_0 < q_1$ . According to the definition of  $q_0$  and  $q_1$ , we must have  $F_0(q) < 1 - \alpha$  and  $F_1(q) < 1 - \alpha$ , so

$$F_S(q) = (1 - p)F_0(q) + pF_1(q) < (1 - p)(1 - \alpha) + p(1 - \alpha) = 1 - \alpha.$$

However, the above derivation of  $F_S(q) < 1 - \alpha$  contradicts the definition of  $q$ , which requires  $F_S(q) \geq 1 - \alpha$ . Therefore, we must have  $q \geq q_0$ . Regarding  $q_1$ , we have

$$F_S(q_1) = (1 - p)F_0(q_1) + pF_1(q_1) \geq (1 - p)(1 - \alpha) + p(1 - \alpha) = 1 - \alpha.$$

Thus,  $q_1 \in \{t \in \mathbb{R} : F_S(t) \geq 1 - \alpha\}$ . Because  $q = \inf\{t \in \mathbb{R} : F_S(t) \geq 1 - \alpha\}$ , we have  $q \leq q_1$ . Together with  $q \geq q_0$ , we have  $q \in [q_0, q_1]$ .  $\square$

## Proof of Theorem 5

**Theorem 5.** (Two-group product-type uncertainty relation) Suppose Assumption 5 holds. Let  $q_0 < q_1$ . Then

$$\omega_u \geq B_{01}, \quad (24)$$

$$\omega_o \geq \rho B_{01}, \quad (25)$$

$$\omega_u \omega_o \geq \rho B_{01}^2. \quad (26)$$

*Proof.* Let  $d_0 := q - q_0 \geq 0$  and  $d_1 := q_1 - q \geq 0$ , so  $d_0 + d_1 = \Delta$ . By the fundamental theorem of calculus and Assumption 5,

$$\omega_o = F_0(q) - F_0(q_0) = \int_{q_0}^q f_0(t) dt \geq m_0 d_0, \quad \omega_u = F_1(q_1) - F_1(q) = \int_q^{q_1} f_1(t) dt \geq m_1 d_1.$$

The relationship (22) gives  $(1-p)m_0d_0 \leq (1-p)\omega_o = p\omega_u$ , while  $\omega_u \geq m_1d_1$ . A convenient way to combine the constraints is to express  $d_0$  in terms of  $\omega_u$ :  $(1-p)\omega_o = p\omega_u$  and  $\omega_o \geq m_0d_0$  imply  $(1-p)m_0d_0 \leq p\omega_u$ , so  $d_0 \leq \frac{p}{(1-p)m_0}\omega_u$ . Similarly,  $\omega_u \geq m_1d_1$  implies  $d_1 \leq \frac{1}{m_1}\omega_u$ . Since  $\Delta = d_0 + d_1$ , we obtain

$$\Delta \leq \left( \frac{1}{m_1} + \frac{p}{1-p} \frac{1}{m_0} \right) \omega_u,$$

which yields (24). Then (25) follows from (22). Multiplying (24) and (25) gives (26).  $\square$

### Proof of Theorem 6

**Theorem 6.** (Generalization of a product-type uncertainty relation)

Suppose Assumption 6 holds. Then

1.  $\max\{\Omega_o(q), \Omega_u(q)\} \geq B_K$  and  $\min\{\Omega_o(q), \Omega_u(q)\} \geq (B_K - |\delta(q)|)_+$ , where  $(x)_+ = \max\{x, 0\}$ .
2.  $\Omega_o(q) \Omega_u(q) \geq B_K (B_K - |\delta(q)|)_+$ .
3. Under exact conservation,  $\delta(q) = 0$ , we have  $\Omega_o(q) \Omega_u(q) \geq B_K^2$ .

*Proof.* For any group with  $q \geq q_g$ , we have  $\varepsilon_g(q) \geq m_g(q - q_g)$ . Similarly, for any group with  $q \leq q_g$ , we have  $\varepsilon_g(q) \leq m_g(q - q_g)$ . Therefore, we have

$$\Omega_o(q) \geq \sum_g w_g(q - q_g)_+ =: A_+(q) \quad \Omega_u(q) \geq \sum_g w_g(q_g - q)_+ =: A_-(q). \quad (37)$$

At the crossing point  $\bar{q}_m$ ,

$$A_+(\bar{q}_m) = A_-(\bar{q}_m) = \frac{1}{2} \sum_g w_g |q_g - \bar{q}_m| = B_K. \quad (38)$$

Since  $A_+(q) - A_-(q) = \sum_{g \in \mathcal{G}} w_g(q - q_g)$ , the two functions cross at  $\bar{q}_m$ . Moreover,  $A_+(q)$  is non-decreasing in  $q$  and  $A_-(q)$  is non-increasing in  $q$ . Hence, the minimum of  $\max\{A_+(q), A_-(q)\}$  is attained at the crossing point, which equals  $B_K$ . Thus, we obtain  $\max\{\Omega_o(q), \Omega_u(q)\} \geq B_K$ . Furthermore, Theorem 1 gives  $\Omega_o(q) - \Omega_u(q) = \delta(q)$ . Since  $\max\{\Omega_o(q), \Omega_u(q)\} - \min\{\Omega_o(q), \Omega_u(q)\} = |\delta(q)|$ , we also have  $\min\{\Omega_o(q), \Omega_u(q)\} \geq (B_K - |\delta(q)|)_+$ . Therefore,

$$\Omega_o(q) \Omega_u(q) \geq B_K (B_K - |\delta(q)|)_+. \quad (39)$$

Under exact conservation,  $\delta(q) = 0$ , and hence

$$\Omega_o(q) \Omega_u(q) \geq B_K^2. \quad (40)$$

$\square$

### Proof of Theorem 7

**Theorem 7.** Suppose Assumption 1 holds. With Definition 2,

$$\sqrt{\mathbb{E}[\varepsilon_G(q)^2]} \cdot L(q) \geq \mathbb{E}[(q - q_G)^2] \geq \sigma_\Delta^2. \quad (31)$$

*Proof.* Let  $Q := q - q_G$ . For groups with  $q \neq q_g$ , (29) implies  $\varepsilon_G(q) = \bar{f}_{S|G}(q) \cdot Q$  almost surely. Then  $\mathbb{E}[Q^2] = \mathbb{E}[\varepsilon_G(q) \cdot \frac{Q}{\bar{f}_{S|G}(q)}]$ . Applying Cauchy–Schwarz yields  $\mathbb{E}[Q^2]^2 \leq \mathbb{E}[\varepsilon_G(q)^2] \cdot \mathbb{E}[(\frac{Q}{\bar{f}_{S|G}(q)})^2]$ . Taking square roots gives the first inequality in (31). The second inequality is identical to the argument in Theorem 2.  $\square$

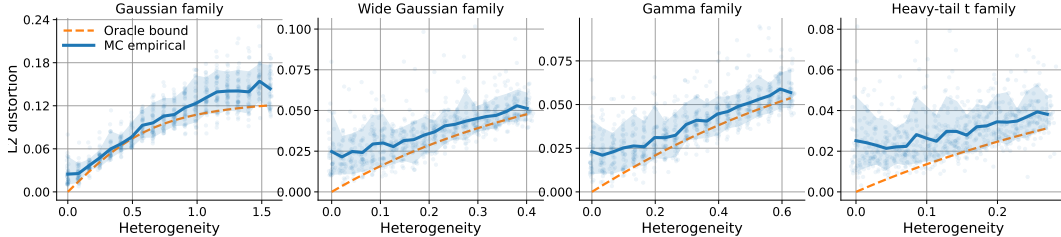


Figure 6: Four multi-group families. Across all four score families, the empirical RMS miscoverage increases with heterogeneity and remains above the lower-bound scale from Theorem 2.

Table 2: Summary of empirical-oracle comparison at the largest heterogeneity value in each setting (means over 40 seeds). Ratios are computed from unrounded means.

Settings	Empirical	Oracle	Ratio
Two-group Gaussian	0.097	0.085	1.141
Four-group Gaussian	0.144	0.121	1.190
Four-group wide Gaussian	0.051	0.048	1.063
Four-group Gamma	0.057	0.054	1.056
Four-group heavy-tail $t$	0.038	0.031	1.226
Coverage $\rightarrow$ size	2.860	2.127	1.345
Size $\rightarrow$ coverage	0.352	0.347	1.014

## C Additional Synthetic Experimental Details

### C.1 Synthetic Simulations

In this experiment, we directly synthesize nonconformity scores, rather than computing them from data and a model. For each group, we estimate the split-conformal threshold by the empirical  $1 - \alpha$  quantile of the calibration scores. The pooled threshold  $\hat{q}$  is obtained by concatenating all calibration scores across subgroups and applying the same quantile rule. Empirical coverage quantities are then evaluated on an independent test sample, so the observed distortion reflects finite-sample threshold estimation.

Figure 6 provides additional pooled-threshold validation. Across the two-group sweep and the four multi-group families, the empirical RMS miscoverage increases with heterogeneity and remains above the oracle scale  $m_{\text{eff}}(q)\sigma_{\Delta}$ . Table 2 reports the empirical-oracle comparison at the largest heterogeneity value in each setting. Table 3 provides details about the distributions of the simulations.

For the set-size based experiments, we use the monotone linear proxy  $\ell_g(t) = a_g + b_g t$ , with  $a_g = 2 + 0.15(g - 1)$  and  $b_g = 0.8 + 0.1(g - 1)$  after labeling the group index as  $g = 1, \dots, K$ . In the size-to-coverage experiment, the common target size is the weighted average of the coverage-calibrated group sizes, namely  $\hat{\lambda} = \sum_g p_g \ell_g(\hat{q}_g)$ , and the equalized-size threshold  $\hat{\tau}_g$  solves  $\ell_g(\hat{\tau}_g) = \hat{\lambda}$ .

### C.2 Imbalance Bottleneck and Ratio Diagnostics

As an additional diagnostic beyond the balanced synthetic experiments, we perform pooled-threshold simulations in four imbalanced settings: Gaussian, wide Gaussian, gamma, and Student- $t$  distributions. Each setting has four distributions of the same type but with imbalanced group masses  $p = (0.60, 0.25, 0.10, 0.05)$ . We use a total calibration budget of  $n_{\text{cal}} = 400$ , 4000 test points per group, target level  $\alpha = 0.1$ , and 40 Monte Carlo seeds. Figure 7 shows that the RMS pooled distortion remains above the oracle scale of all four families, whereas the minority-group absolute gap grows more rapidly with heterogeneity. To verify that the bottleneck is indeed concentrated on the rarest group, Table 5 reports how often the minority group is the largest-gap group for each heterogeneity level. The entries report counts out of 40 seeds for which the minority group attains the largest absolute gap. The frequency rises rapidly with heterogeneity and reaches 40/40 at the largest heterogeneity of 2.0. This pattern indicates a clear minority bottleneck under pooled calibration.

Table 3: Simulation setups for the pooled-threshold experiments in Figure 2 and Figure 6. All groups have equal weight  $p_g = 1/K$ , all experiments use  $\alpha = 0.1$ , and the empirical miscoverage is compared against the theoretical scale  $m_{\text{eff}}(q)\sigma_\Delta$ .

Setting	Score family	Cal/Test
Two-group Gaussian shift	$S \mid G = g \sim \mathcal{N}(\mu_g, 1)$ , with $(\mu_0, \mu_1) = (0, \delta)$ and $\delta \in [0, 2]$	50/500
Four-group Gaussian shift	$S \mid G = g \sim \mathcal{N}(\mu_g, 1)$ , with $\mu_g = s(-1.5, -0.5, 0.5, 1.5)$ and $s \in [0, 1.4]$	50/500
Four-group wide Gaussian	$S \mid G = g \sim \mathcal{N}(0, \sigma_g^2)$ , with $\sigma_g = 1 + s(0, 0.2, 0.4, 0.6)$ and $s \in [0, 1.4]$	50/500
Four-group Gamma	$S \mid G = g \sim \text{Gamma}(4, \theta_g)$ , with $\theta_g = 0.55 + s(0, 0.06, 0.12, 0.18)$ and $s \in [0, 1.4]$	50/500
Four-group heavy-tail $t$	$S \mid G = g \sim t_6(0, \sigma_g)$ , with $\sigma_g = 0.9 + s(0, 0.12, 0.24, 0.36)$ and $s \in [0, 1.4]$	50/500

Table 4: Simulation setups for the group-adjusted trade-off experiments in Figure 1. All groups have equal weight  $p_g = 1/K$  and all experiments use  $\alpha = 0.1$ .

Setting	Score family	Cal/Test	Compared quantity
Coverage vs. size	Two-component asymmetric Gaussian mixtures with group-specific offsets, scales, and weights; $s \in [0, 1.8]$ scales group centers and increases quantile separation	25/100	size change vs. $v_{\text{eff}}(q)\sigma_\Delta$
Size vs. coverage	Two-component mixtures of one Student- $t$ component and one Gaussian component, with group-specific offsets, scales, and weights; $s \in [0, 2.0]$ scales group centers	25/100	coverage change vs. $\kappa_{\text{eff}}(\lambda)\sigma_\lambda$

Tables 6 and 7 record empirical and oracle ratios for the two policy-conversion diagnostics at selected heterogeneity levels. The coverage-to-size ratio remains above one throughout, with the finite-sample slack shrinking as  $n_{\text{cal}}$  grows. The size-to-coverage ratio is tighter and concentrates near one much more quickly.

## D Bias in Bios Experiments

### D.1 Experimental Settings

We perform conformal analysis on outputs from a DistilBERT<sup>3</sup> classifier trained on the ten most frequent professions from Bias in Bios<sup>4</sup>. Training uses cleaned, preprocessed text with a maximum sequence length of 160, a learning rate of  $2 \times 10^{-5}$ , weight decay of 0.01, batch sizes of 64/32 for training/validation, warm-up ratio 0.05, and two training epochs. The validation accuracy

<sup>3</sup>We use the Hugging Face checkpoint `distilbert-base-uncased`; model card: <https://huggingface.co/distilbert/distilbert-base-uncased>. The model card lists the license as Apache-2.0.

<sup>4</sup>We use the Hugging Face dataset `LabHC/bias_in_bios`; dataset card: [https://huggingface.co/datasets/LabHC/bias\\_in\\_bios](https://huggingface.co/datasets/LabHC/bias_in_bios). The dataset card lists the license as MIT. For the original dataset source, see [6].

Table 5: Minority frequency across heterogeneity levels.

Family	Heterogeneity level				
	0.0	0.5	1.0	1.5	2.0
Gaussian	13/40	40/40	40/40	40/40	40/40
Wide Gaussian	13/40	36/40	39/40	40/40	40/40
Gamma	13/40	37/40	40/40	40/40	40/40
Heavy-tail $t$	9/40	30/40	39/40	37/40	40/40

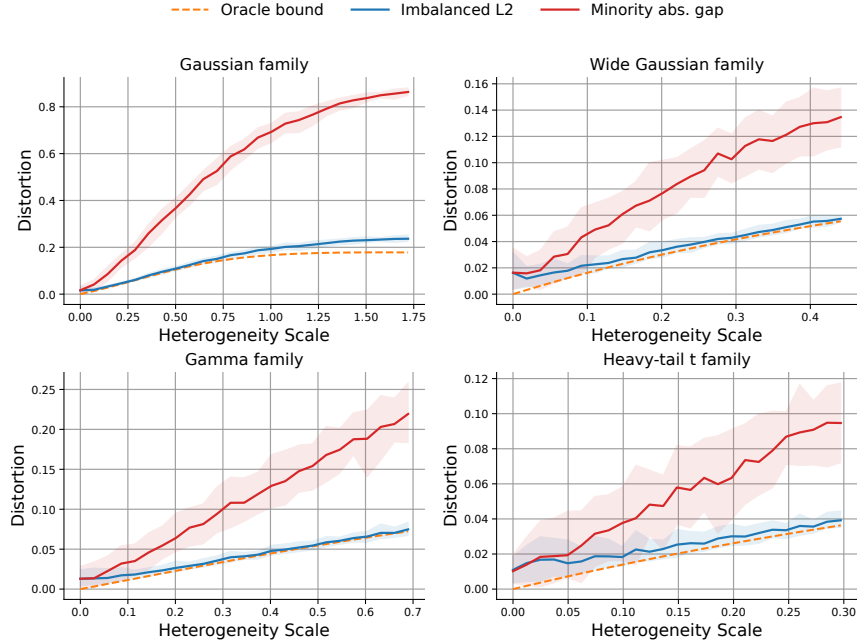


Figure 7: Imbalanced four-group pooled-threshold diagnostics. Across all four families, the weighted RMS distortion remains above the lower-bound scale from Theorem 2. At the same time, the minority-group absolute gap grows more rapidly with heterogeneity, showing that pooled distortion can concentrate on rare groups.

Table 6: Coverage-to-size empirical/oracle ratio at heterogeneity levels  $\sigma_\Delta$ .

$n_{\text{cal}}$	Selected heterogeneity level $\sigma_\Delta$				
	0.378	0.855	1.250	1.652	2.192
12	1.837	1.417	1.327	1.334	1.392
25	1.443	1.174	1.243	1.244	1.296
50	1.284	1.174	1.178	1.232	1.287
100	1.226	1.087	1.172	1.227	1.305
200	1.086	1.085	1.161	1.210	1.298
400	1.034	1.068	1.139	1.218	1.293

and macro-F1 score are 0.8886 and 0.8569, respectively. The dataset is partitioned into training, validation, calibration, and test splits of sizes 185758, 20640, 31764, and 79397, with stable group balance across splits. Details are provided in Table 9. Throughout, we use the simple score in the main presentation, while SAPS and RAPS are included to show that the same conclusions are not specific to a single score construction. Detailed per-group values for the simple score are shown in Table 8.

Table 7: Size-to-coverage empirical/oracle ratio at heterogeneity levels  $\sigma_\Delta$ .

$n_{\text{cal}}$	Selected heterogeneity level $\sigma_\Delta$				
	0.437	0.741	1.201	1.862	2.369
12	1.313	1.181	1.028	1.087	1.038
25	1.095	1.025	1.009	0.990	1.012
50	0.981	0.994	0.997	1.001	0.994
100	1.002	0.997	0.987	1.003	1.002
200	1.019	1.009	1.003	0.999	1.004
400	1.017	1.002	0.996	1.004	1.004

Table 8: Summary for Bias in Bios at  $\alpha = 0.10$  for the simple score.

Quantity	Group (Male)	Group (Female)
$p_g$	0.5275	0.4725
$q_g$	0.6298	0.6531
$\varepsilon_g(q)$	0.0020	-0.0009
$\lambda_g = \ell_g(q_g)$	1.0140	1.0231
$\ell_g(q_g) - \ell_g(q)$	-0.0050	0.0053
$\tau_g$	0.6410	0.6430
$\hat{F}_{S g}(\tau_g) - \hat{F}_{S g}(q_g)$	0.0016	-0.0018

Table 9: Split sizes and group composition for Bias in Bios.

Split	Total $n$	Group 0 (Male)	Group 1 (Female)
Model train	185,758	97,985 (52.75%)	87,773 (47.25%)
Model validation	20,640	10,886 (52.74%)	9,754 (47.26%)
Calibration	31,764	16,755 (52.75%)	15,009 (47.25%)
Test	79,397	41,881 (52.75%)	37,516 (47.25%)

## D.2 Robustness across Target Coverage

We vary the target miscoverage level over  $\alpha \in \{0.05, 0.07, 0.085, 0.10\}$  and keep the rest of the pipeline unchanged across three score families. The simple score gives the baseline pattern, while the same trade-off is preserved under SAPS and RAPS. Tables 10, 11 and 12 report the  $\alpha$ -robustness summaries for simple, SAPS and RAPS.

## D.3 Controlled Group Temperature Sweep

In this section, we construct a controlled heterogeneity view at the fixed target level  $\alpha = 0.1$  by temperature scaling the class probability vector of group 1 through a specific temperature  $T \in \{1.00, 1.10, 1.25, 1.50, 1.75, 2.00\}$  and renormalizing  $p^{1/T}$ . Adjusting the temperature parameter amplifies the same mechanism shown at the baseline. Parallel to the previous section, we present the simple, SAPS, and RAPS scores under temperature sweep, showing a score-robust conversion pattern in Tables 13, 14, and 15.

## D.4 Robustness to Alternative Scores

The same conversion mechanism is also visible under the SAPS and RAPS scores. Table 16 shows that all three scores exhibit the same pattern: pooled threshold coverage discrepancy, nonzero set size distortion after applying the group-wise thresholds  $q_g$ , and nonzero coverage distortion after imposing an equalized set size.

## D.5 Finite Calibration of the Pooled-Threshold Floor

This section complements the population uncertainty relations in Section 3, where the pooled-threshold floor obeys

$$\|\varepsilon(q)\|_{L^2(p)} \geq m_{\text{eff}}(q) \sigma_{\Delta}, \quad (41)$$

where  $q$  is the pooled threshold,  $q_g$  are the group-specific  $1 - \alpha$  quantiles, and  $\sigma_{\Delta} = \text{sd}(q_G)$ . The question here is finite-sample rather than population-level: how large must the calibration split be before the structural floor in Equation (41) becomes empirically resolvable under split conformal calibration?

We fix the trained model outputs and vary only the calibration size. For each score choice (simple, SAPS, RAPS), we repeatedly form group-stratified subsamples of the original calibration split, recompute the pooled conformal threshold  $\hat{q}_n$ , and evaluate the resulting RMS group miscoverage on a fixed test set. Throughout, we set the target level  $\alpha = 0.1$  and the number of groups  $K = 2$ , and we use 300 subsamples for each

$$n \in \{200, 500, 1000, 2000, 4000, 7000, 15000, 20000, 25000, 28000\}.$$

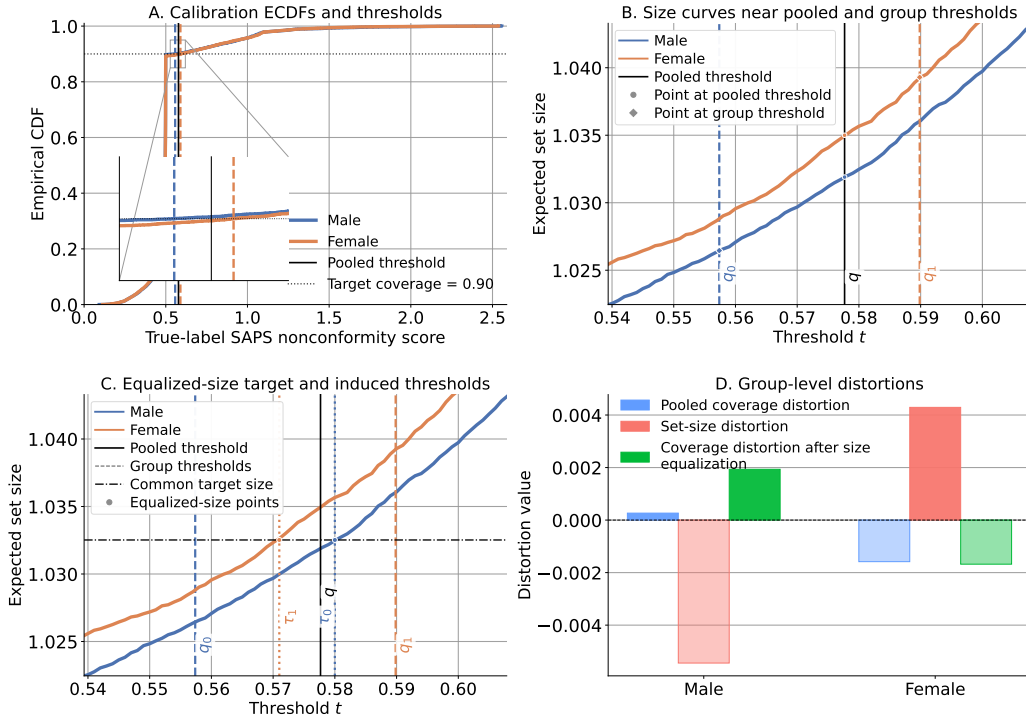


Figure 8: Bias in Bios mechanism view at  $\alpha = 0.10$  for SAPS score. Panel A illustrates the pooled-threshold mechanism in Theorem 1; Panels B–C illustrate Theorems 3–4 and Corollaries 1–2; Panel D summarizes the three distortions for male and female groups.

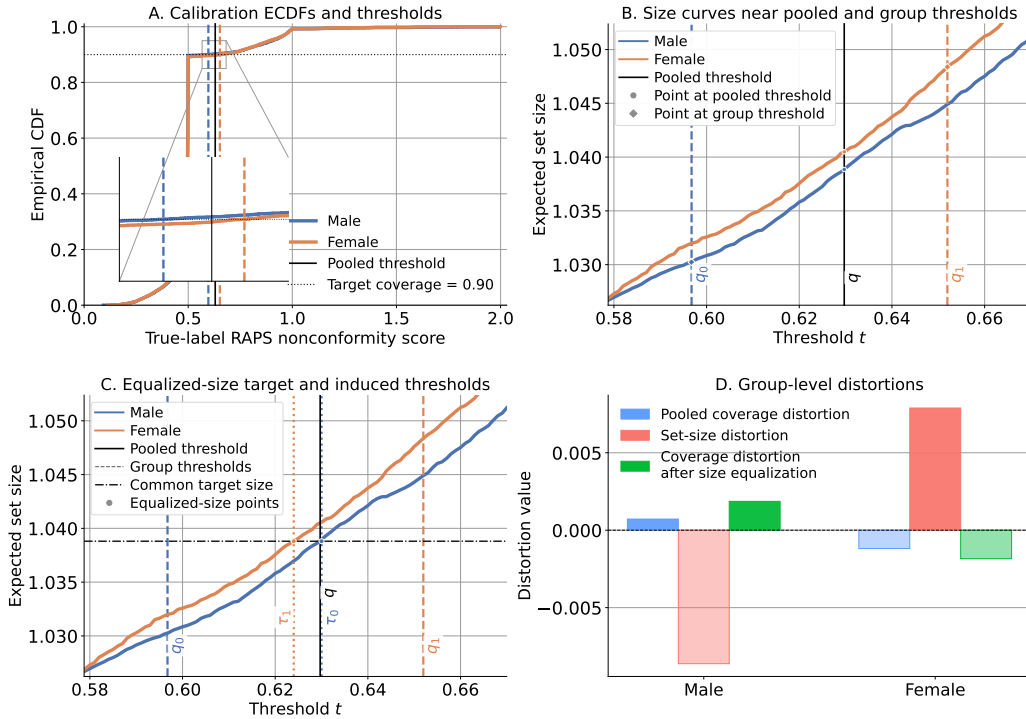


Figure 9: Bias in Bios mechanism view at  $\alpha = 0.10$  for RAPS score. Panel A illustrates the pooled-threshold mechanism in Theorem 1; Panels B–C illustrate Theorems 3–4 and Corollaries 1–2; Panel D summarizes the three distortions for male and female groups.

Table 10:  $\alpha$ -robustness for the simple score.

$\alpha$	$\sigma_\Delta$	RMS pooled coverage	RMS size deviation from $q_g$	RMS coverage after equalized size
0.050	$4.60 \times 10^{-5}$	0.0021	0.0002	0.0006
0.070	0.0019	0.0005	0.0017	0.0014
0.085	0.0054	0.0005	0.0035	0.0016
0.100	0.0116	0.0015	0.0051	0.0017

Table 11:  $\alpha$ -robustness for SAPS.

$\alpha$	$\sigma_\Delta$	RMS pooled coverage	RMS size deviation from $q_g$	RMS coverage after equalized size
0.050	0.0039	0.0011	0.0047	0.0005
0.070	0.0022	0.0009	0.0019	0.0008
0.085	0.0015	0.0007	0.0009	0.0013
0.100	0.0162	0.0011	0.0049	0.0018

Let  $q^*$  denote the pooled threshold computed from the full test set, used as a population proxy. We then define

$$\text{floor}^* := \left( \sum_{g=1}^K p_g^{\text{test}} \varepsilon_g(q^*)^2 \right)^{1/2}, \quad \widehat{\text{floor}}(n) := \left( \sum_{g=1}^K p_g^{\text{test}} \varepsilon_g(\hat{q}_n)^2 \right)^{1/2},$$

and summarize the signal-to-noise ratio by  $\text{SNR}(n) := \frac{\text{floor}^*}{\text{sd}(\widehat{\text{floor}}(n))}$ . We interpret  $\text{SNR}(n) \geq 1$  as the point where the structural floor is at least as large as the calibration-induced standard deviation.

For the empirical estimation, the stiffness factor  $m_{\text{eff}}(q)$  is replaced by a local density proxy at  $q^*$ , estimated from the pooled test scores by a window

$$\widehat{m}_{\text{eff}}(q^*) := \frac{1}{2hn_{\text{test}}} \sum_{i=1}^{n_{\text{test}}} \mathbf{1}\{|S_i - q^*| \leq h\},$$

with a Silverman-type [23] bandwidth  $h = 0.9 \hat{\sigma}_{\text{rob}} n_{\text{test}}^{-1/5}$ ,  $\hat{\sigma}_{\text{rob}} = \min(\hat{\sigma}, \text{IQR}/1.34)$ , where  $n_{\text{test}}$  is the test set size and  $\hat{\sigma}$  is the standard deviation of test scores. Then, the estimated stiffness factor  $\widehat{m}_{\text{eff}}(q^*)$  serves as an empirical detectability proxy for the local CDF slope entering Equation (41), not as an exact plug-in estimate of the group-specific quantity in Definition 1.

To motivate the detectability scale, we use a DKW-style empirical-CDF heuristic [7], treating the calibration scores within each group as IID. Under an infinitely exchangeable model, this IID step can also be read conditionally on the de Finetti directing measure [9]. This is stronger than the exchangeability assumption needed for CP and is used only for the sample-size diagnostic below. If  $n$  denotes the total calibration size and the groups are roughly balanced, each group has about  $n/K$  calibration scores. A union bound over the  $K$  group-wise empirical CDFs gives a uniform fluctuation scale of order

$$\sqrt{\frac{\log(K/\xi)}{n/K}} = \sqrt{\frac{K \log(K/\xi)}{n}}. \quad (42)$$

After quantile inversion, the corresponding threshold-noise scale is of order  $\sqrt{\frac{K \log(K/\xi)}{n m_{\text{eff}}(q)^2}}$ . Requiring this noise scale to be no larger than the intrinsic quantile separation scale  $\sigma_\Delta$  motivates

$$n \gtrsim \frac{K \log(K/\xi)}{m_{\text{eff}}(q)^2 \sigma_\Delta^2}, \quad (43)$$

where  $K$  is the number of groups and  $\xi$  is a fixed confidence parameter. We choose  $K = 2$  and  $\xi = 0.05$  in the plots across the score choices.

Panels A–B of Figure 10 show a clear signal-resolution transition. The mean empirical floor decreases monotonically with  $n$ , while the detectability ratio rises steadily and crosses the  $\text{SNR}(n) = 1$

Table 12:  $\alpha$ -robustness for RAPS.

$\alpha$	$\sigma_\Delta$	RMS pooled coverage	RMS size deviation from $q_g$	RMS coverage after equalized size
0.050	0.0055	0.0018	0.0121	0.0002
0.070	0.0005	0.0013	0.0008	0.0013
0.085	0.0007	0.0003	0.0006	0.0006
0.100	0.0276	0.0010	0.0083	0.0019

Table 13: Bias in Bios temperature sweep for the simple score at  $\alpha = 0.10$ .

$T$	$\sigma_\Delta$	RMS pooled coverage	RMS size from $q_g$	RMS coverage after equalized size
1.00	0.0116	0.0015	0.0051	0.0017
1.10	0.0136	0.0018	0.0061	0.0015
1.25	0.0169	0.0027	0.0083	0.0015
1.50	0.0241	0.0044	0.0126	0.0015
1.75	0.0346	0.0067	0.0205	0.0022
2.00	0.0432	0.0088	0.0275	0.0028

threshold first for the simple score, and on the  $1.5 \times 10^4$  scale for both SAPS and RAPS. The order matches Equation (43). In particular, the score with the steepest local CDF near  $q$  requires the fewest calibration points to resolve the floor.

Panels C–D of Figure 10 show that small calibration sets do not merely add variance. They also inflate both the observed lower bound and the empirical heterogeneity estimate  $\hat{\sigma}_\Delta$ , so limited calibration size may exaggerate the lower bound.

Finally, let

$$C_{\text{det}} := \frac{n_{\text{detect}} m_{\text{eff}}(q)^2 \sigma_\Delta^2}{K \log(K/\xi)}, \quad \xi = 0.05.$$

Here,  $m_{\text{eff}}(q)$  is the local density proxy at the pooled test-proxy threshold,  $\sigma_\Delta$  is the test-proxy heterogeneity of the group quantiles,  $\text{floor}^*$  is the true-floor proxy, and  $n_{\text{detect}}$  is the smallest calibration size with  $\text{SNR}(n) \geq 1$ . Table 17 shows that  $C_{\text{det}}$  is stable across all three scores up to a common multiplicative scale, which serves as a diagnostic of detectability.

In summary, Section 3 identifies a population lower bound driven by intrinsic heterogeneity  $\sigma_\Delta$  and local stiffness  $m_{\text{eff}}(q)$ . The present experiments show that observing the lower bound in finite-sample split conformal calibration is itself a sample-size-related phenomenon. Empirically, the relevant resolution scale is well summarized by  $m_{\text{eff}}(q)^2 \sigma_\Delta^2$ . That is, once  $n$  is large enough relative to the inverse of the resolution scale, the lower bound becomes detectable and the empirical curves stabilize near the population proxy.

Table 14: Bias in Bios temperature sweep for SAPS at  $\alpha = 0.10$ .

$T$	$\sigma_{\Delta}$	RMS pooled coverage	RMS size from $q_g$	RMS coverage after equalized size
1.00	0.0162	0.0011	0.0049	0.0018
1.10	0.0058	0.0009	0.0018	0.0020
1.25	0.0086	0.0015	0.0024	0.0020
1.50	0.0315	0.0028	0.0077	0.0067
1.75	0.0396	0.0056	0.0128	0.0063
2.00	0.0489	0.0107	0.0226	0.0107

Table 15: Bias in Bios temperature sweep for RAPS at  $\alpha = 0.10$ .

$T$	$\sigma_{\Delta}$	RMS pooled coverage	RMS size from $q_g$	RMS coverage after equalized size
1.00	0.0276	0.0010	0.0083	0.0019
1.10	0.0121	0.0004	0.0034	0.0020
1.25	0.0080	0.0013	0.0024	0.0020
1.50	0.0355	0.0033	0.0098	0.0022
1.75	0.0584	0.0045	0.0150	0.0086
2.00	0.0683	0.0093	0.0248	0.0076

Table 16: Bias in Bios comparison across three scores at  $\alpha = 0.10$ .

Score	$q$	$\sigma_{\Delta}$	RMS pooled coverage	RMS size from $q_g$	RMS coverage after equalized size
Simple	0.6423	0.0116	0.0015	0.0051	0.0017
SAPS	0.5777	0.0162	0.0011	0.0049	0.0018
RAPS	0.6297	0.0276	0.0010	0.0083	0.0019

Table 17: Detectability summary at  $\alpha = 0.1$ .

Score	$m_{\text{eff}}(q)$	$\sigma_{\Delta}$	floor*	full-calibration floor	$n_{\text{detect}}$	$C_{\text{det}}$
RAPS	0.0564	0.0139	0.0010	0.0010	15000	0.0013
SAPS	0.0672	0.0094	0.0009	0.0011	15000	0.0008
Simple	0.1581	0.0094	0.0015	0.0016	7000	0.0021

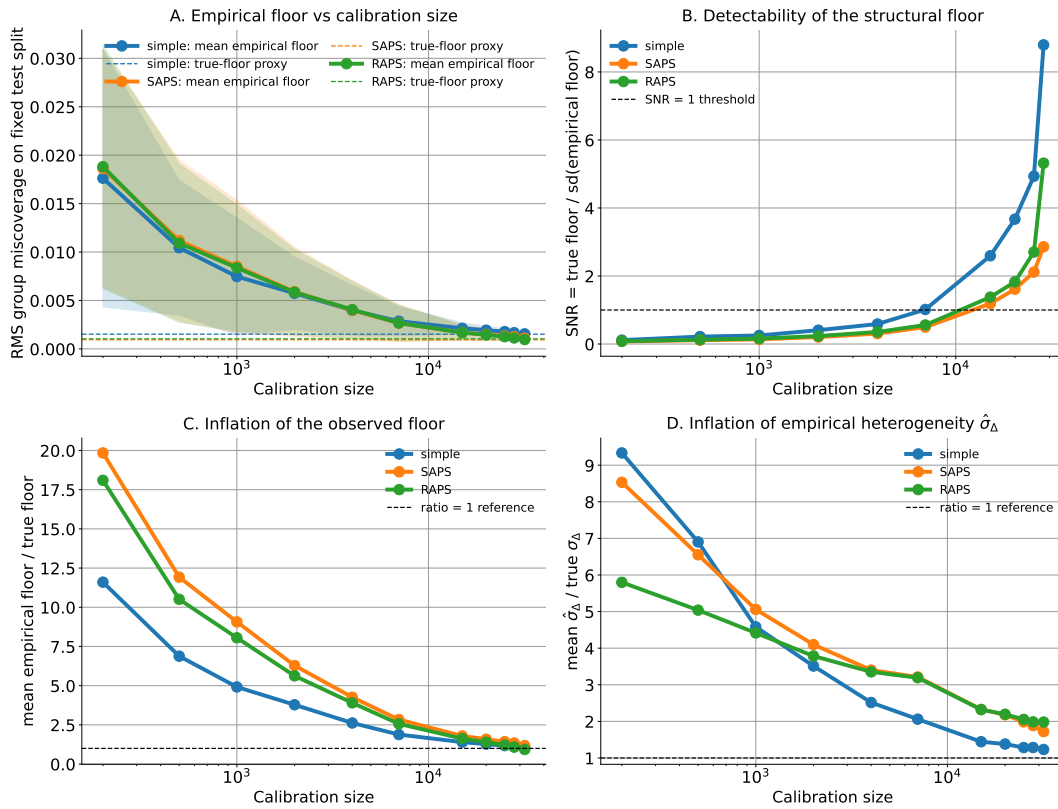


Figure 10: Finite-calibration detectability diagnostics of the pooled-threshold floor from Theorem 2 on Bias in Bios. Panels A–B show how the empirical floor and its detectability improve with the calibration size. The dashed line at  $\text{SNR}(n) = 1$  marks the empirical detectability benchmark. Panels C–D show that small calibration splits can also inflate the observed floor and estimated heterogeneity.

## E MultiNLI Experiments

### E.1 Experiment Settings

All post-hoc quantities are defined exactly as in Section 5.2 except for the dataset-specific details. We use the Hugging Face MultiNLI corpus<sup>5</sup>, treat the ten genres as groups, and train a DistilBERT classifier for three-class NLI. The run uses a maximum sequence length of 256, a learning rate of  $2 \times 10^{-5}$ , a weight decay of 0.01, batch sizes of 64/32, a warm-up ratio of 0.05, and two epochs. The validation accuracy and macro-F1 are 0.8104 and 0.8100. The detailed split sizes and the summary of the key quantities are shown in Tables 18 and 19. In addition, Table 20 reports the full per-genre quantities at level  $\alpha = 0.1$ . The alternative score results for SAPS and RAPS are deferred to Section E.4.

### E.2 Robustness across Target Coverage

Figure 11 shows that across  $\alpha \in \{0.05, 0.07, 0.085, 0.1\}$ , the empirical pooled-threshold distortion stays above the estimated lower-bound scale, while the induced size and coverage distortions remain nonzero throughout.

### E.3 Controlled Genre Temperature Sweep

At  $\alpha = 0.1$ , we perturb only the facetoface genre via temperature scaling. Figure 12 shows that across the sweep, the empirical pooled-threshold distortion remains above the estimated lower bound, and the induced size and coverage distortions stay nonzero.

### E.4 Alternative Scores

The same mechanism persists under SAPS and RAPS with the model, groups, and split protocol fixed. SAPS uses the default temperature  $T = 1.0$  and  $\lambda_{\text{SAPS}} = 0.3$ ; RAPS uses the default temperature  $T = 0.6$ ,  $k_{\text{reg}} = 1$ , and  $\lambda_{\text{RAPS}} = 0.02$ . Both scores utilize the randomization level  $u = 0.5$ . Figure 13 demonstrates that at  $\alpha = 0.1$ , the SAPS score shows a pooled floor, a nonzero set size distortion after switching from pooled  $q$  to group-wise  $q_g$ , and a nonzero coverage distortion after imposing the equalized expected set size. Robustness checks are provided in Figures 14 and 15. We do not view these results as requiring pointwise lower-bound dominance at every  $\alpha$  or temperature value. For SAPS and RAPS, Panel A is best interpreted as a finite-sample diagnostic based on an estimated lower-bound proxy, while the main evidence remains visible.

<sup>5</sup>Hugging Face dataset: nyu-ml1/multi\_nli; [https://huggingface.co/datasets/nyu-ml1/multi\\_nli](https://huggingface.co/datasets/nyu-ml1/multi_nli). The dataset card states that most of the corpus is released under the OANC license, while the FICTION section includes Creative Commons Attribution 3.0, Creative Commons Share-Alike 3.0, and U.S. public-domain materials.

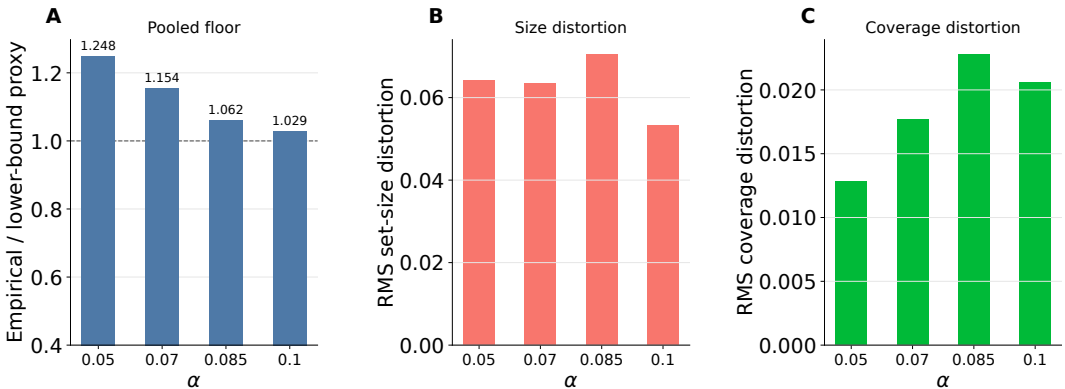


Figure 11: MultiNLI robustness across  $\alpha$  for the simple score. Panel A displays Theorem 2: the empirical pooled-threshold distortion stays near or above the lower-bound scale across the tested  $\alpha$ -grid. Panels B–C illustrate Corollaries 1–2: the induced set-size and coverage distortions remain nonzero throughout.

Table 18: Split sizes for MultiNLI.

Split	$n$
Model train	353,431
Model validation	39,271
Calibration	9,823
Test	9,824

Table 19: Summary for MultiNLI at  $\alpha = 0.10$  with simple score.

$\sigma_\Delta$	RMS pooled coverage	$\lambda$	RMS size distortion	$\sigma_\lambda$	RMS coverage distortion
0.0354	0.0150	1.2717	0.0532	0.0779	0.0209

### E.5 Detectability under Finite Calibration

This subsection follows Appendix D.5 with the same finite calibration protocol. Because MultiNLI has fewer genre-stratified calibration examples than Bias in Bios, we use the grid

$$n \in \{50, 100, 150, 200, 250, 300, 350, 400, 450, 500\}.$$

We fix the trained MultiNLI outputs and test split, vary only the calibration size through genre-stratified subsampling, recompute the pooled threshold on each subsample, and evaluate the resulting RMS genre-wise miscoverage on the fixed test set. Figure 16a shows that the floor becomes visible around  $n = 100$ , and is clearly resolved for all three scores thereafter. Hence, on the MultiNLI dataset, the structural signal is empirically visible once the calibration split is moderately large.

Table 20: Per-genre summary for MultiNLI at  $\alpha = 0.1$  with simple score.

Genre	$p_g$	$q_g$	$\varepsilon_g(q)$	$\lambda_g$	$\lambda_g - \ell_g(q)$	$\tau_g$	$\hat{F}_{S g}(\tau_g) - \hat{F}_{S g}(q_g)$
Government	0.0989	0.7215	0.0198	1.1420	-0.0905	0.8200	0.0463
Letters	0.1006	0.7561	0.0119	1.1741	-0.0304	0.8360	0.0192
Travel	0.1007	0.7747	0.0090	1.2285	-0.0303	0.8030	0.0081
Oup	0.0998	0.7802	0.0082	1.2439	-0.0173	0.8050	0.0051
Verbatim	0.0990	0.8151	0.0044	1.3464	0.0380	0.7730	-0.0195
Fiction	0.1004	0.8371	0.0037	1.3398	0.0659	0.7910	-0.0132
Facetoface	0.1006	0.8223	0.0008	1.3168	0.0506	0.7960	-0.0101
Telephone	0.1001	0.7951	-0.0150	1.3001	0.0020	0.7810	-0.0061
Nineeleven	0.1005	0.7883	-0.0155	1.2249	-0.0091	0.8220	0.0132
Slate	0.0996	0.8410	-0.0329	1.4008	0.0982	0.7750	-0.0307

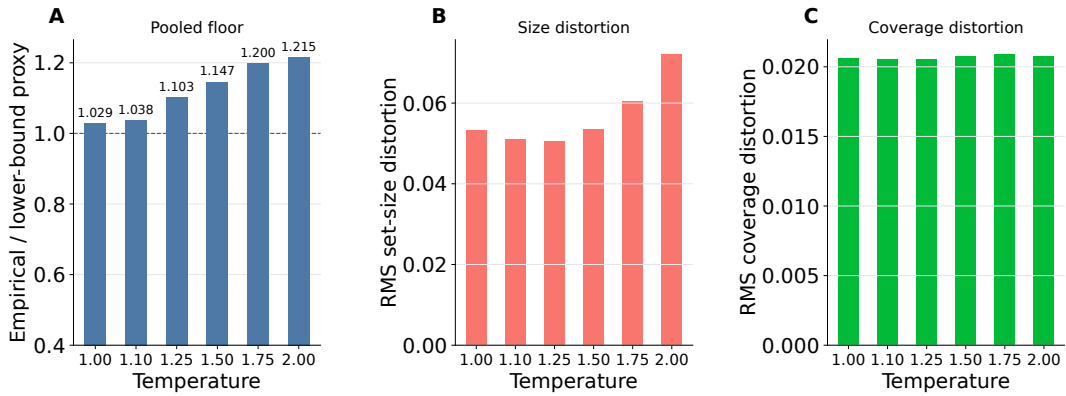


Figure 12: Controlled MultiNLI temperature sweep at  $\alpha = 0.10$  for the simple score, perturbing the *facetoface* genre only. Panel A corresponds to Theorem 2. Panels B–C show Corollaries 1–2. The same trade-off mechanism remains visible across the temperature sweep.

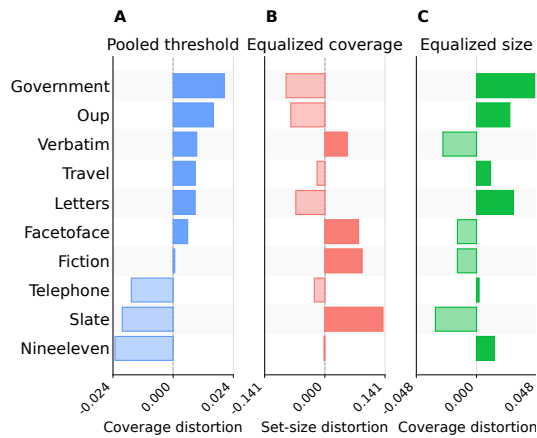


Figure 13: MultiNLI at  $\alpha = 0.10$  using SAPS score. For this score, Panel A shows pooled quantile consequence of Theorem 1; Panels B and C illustrate the set size distortion in Corollary 1, and the coverage distortion in Corollary 2, respectively.

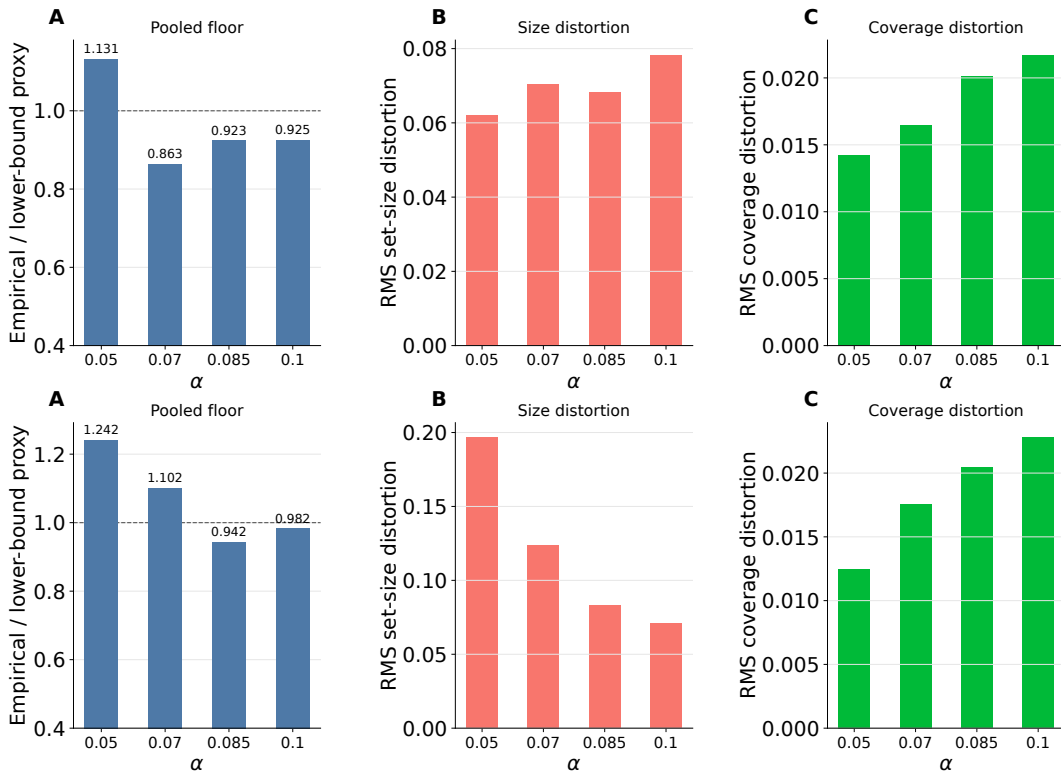


Figure 14: MultiNLI robustness across  $\alpha$  for SAPS (top) and RAPS (bottom) scores. In each row, Panel A is best read as a finite-sample diagnostic for Theorem 2 based on an estimated lower-bound proxy, rather than a pointwise lower-bound verification. Panels B–C show Corollaries 1–2. The induced set-size and coverage distortions remain visible across the tested  $\alpha$ -grid.

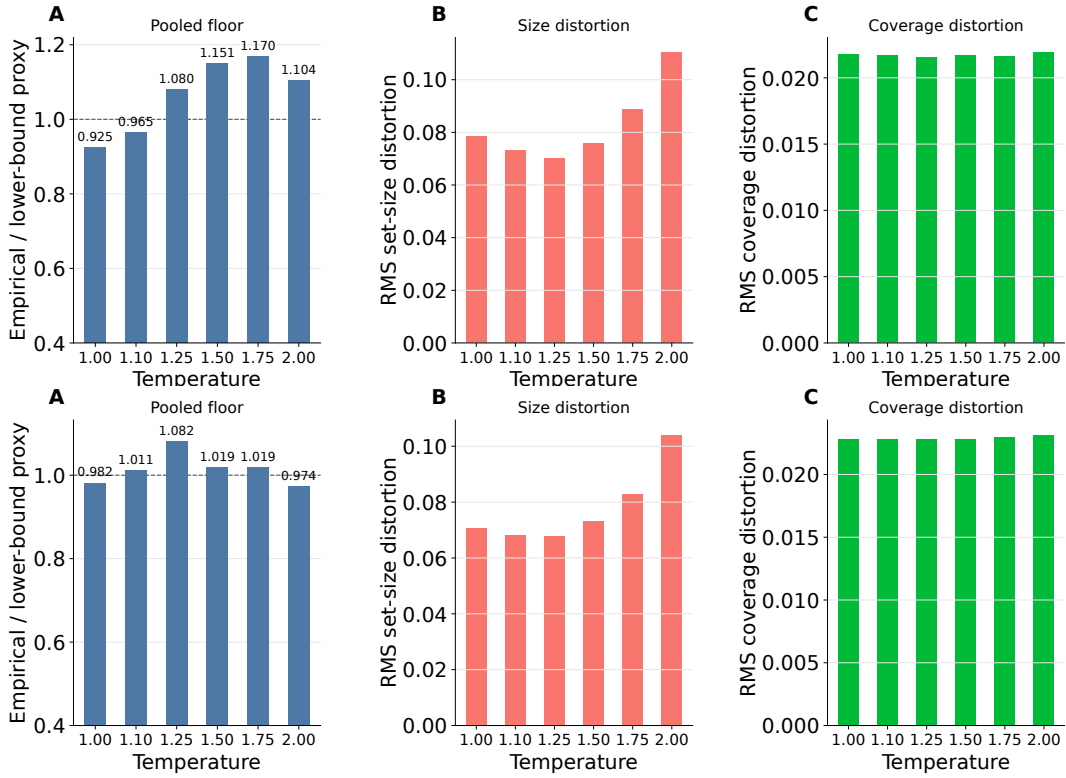


Figure 15: Controlled MultiNLI temperature sweep at  $\alpha = 0.10$  for SAPS (top) and RAPS (bottom) scores, perturbing the *facetoface* genre only. Panel A is best read as a finite-sample diagnostic for Theorem 2. Panels B–C illustrate Corollaries 1–2. The same trade-off mechanism remains visible across the temperature sweep.

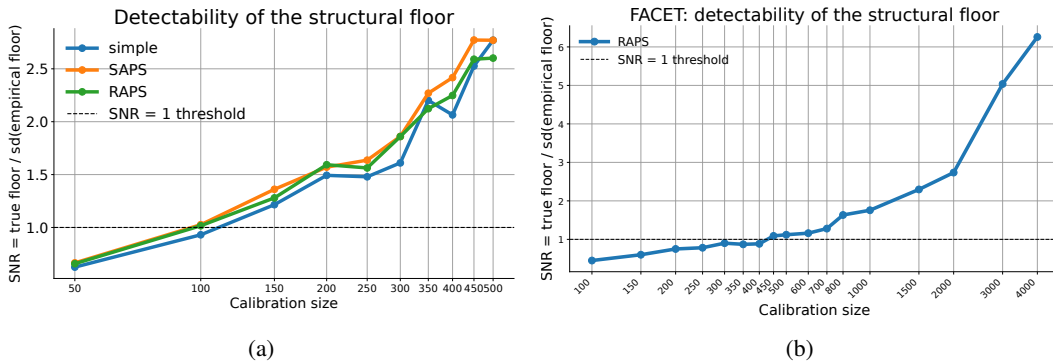


Figure 16: Finite-calibration detectability of the pooled-threshold floor from Theorem 2. Left: MultiNLI, for simple, SAPS, and RAPS scores. Right: FACET, for RAPS score. The dashed line at  $\text{SNR}(n) = 1$  marks the empirical detectability benchmark, so crossing it indicates that the structural floor is becoming distinguishable from finite-sample fluctuation.

## F FACET Experiments

### F.1 Experiment Settings and Summary

For FACET,<sup>6</sup> we use CLIP ViT-L/14.<sup>7</sup> All post-hoc quantities are defined exactly as in Sections 5.2 and 5.3. Tables 21, 22 and 23 list the key quantities, the full per-group quantities, and the experiment configuration, respectively.

### F.2 Robustness across Target Coverage and Temperature Perturbation

Figure 17 shows that for various target levels  $\alpha \in \{0.05, 0.07, 0.085, 0.10\}$ , the empirical pooled-threshold distortion stays above the empirical lower bound. The induced set size distortion remains nonzero throughout and the equalized expected set size policy continues to produce a nonzero RMS coverage distortion.

Next, we perturb only the Younger group through temperature scaling while keeping the rest of the groups fixed. Figure 18 shows that across perturbations, the pooled RMS gap remains at or above the lower bound proxy. The equalized expected set size policy continues to introduce a visible coverage distortion across the sweep.

<sup>6</sup>We use the FACET benchmark dataset released by Meta AI; official dataset page: <https://ai.meta.com/datasets/facet/>. The FACET data card in the ICCV 2023 supplemental material states that the license is “Custom license, see dataset download agreement,” and that FACET is intended for evaluation only. For a description of the benchmark, see [13].  
<sup>7</sup>CLIP ViT-L/14 from OpenAI repository: <https://github.com/openai/CLIP>. The repository LICENSE file states that the code is released under the MIT License.

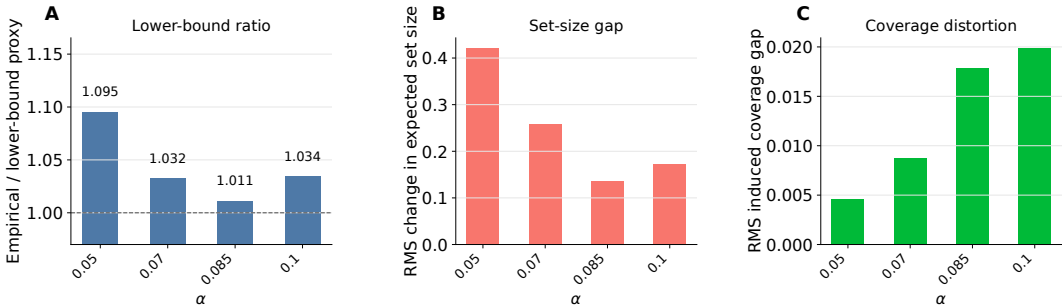


Figure 17: FACET robustness across  $\alpha$  for the RAPS score. Panel A illustrates Theorem 2: the empirical pooled-threshold distortion stays near or above the lower-bound scale across the tested  $\alpha$ -grid. Panels B–C show Corollaries 1–2: the induced set-size and coverage distortions remain nonzero throughout.

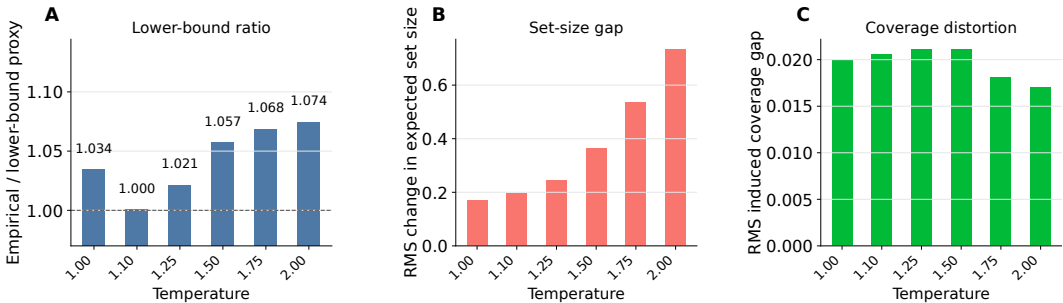


Figure 18: Controlled FACET temperature sweep at  $\alpha = 0.10$  for the RAPS score, perturbing the Younger group only. Panel A evaluates the lower-bound behavior in Theorem 2. Panels B–C show Corollaries 1–2. The same trade-off mechanism remains visible across the temperature sweep.

Table 21: FACET RAPS summary at  $\alpha = 0.10$ .

Metric	Value
$q$	1.0194
$\sigma_\Delta$	0.0040
Pooled RMS	0.0083
Lower bound	0.0080
Ratio	1.034
$\lambda$	2.1735
RMS set size	0.1717
$\sigma_\lambda$	0.2817
RMS coverage	0.0199

Table 22: Per-group quantities for FACET at  $\alpha = 0.1$ .

Age group	$p_g$	$q_g$	$\varepsilon_g(q)$	$\lambda_g$	$\lambda_g - \ell_g(q)$	$\tau_g$	$\hat{F}_{S g}(\tau_g) - \hat{F}_{S g}(q_g)$
Younger	0.1795	1.0177	0.0176	1.8757	-0.0892	1.0200	0.0054
Middle	0.5718	1.0196	-0.0035	2.0921	0.0182	1.0200	0.0025
Older	0.0461	1.0111	-0.0105	1.9895	-0.3421	1.0171	0.0263
Unknown	0.2026	1.0276	-0.0018	2.7090	0.3329	1.0126	-0.0419

### F.3 Detectability under Finite Calibration

Following the detectability analysis in Appendices D.5 and E.5, we fix the model outputs and test split, vary only the calibration sample size through age-stratified subsampling, recompute the pooled threshold on each subsample, and evaluate the resulting RMS group-wise coverage on the fixed test split. For FACET, we use the grid

$$n \in \{100, 150, 200, 250, 300, 350, 400, 450, 500, 600, 700, 800, 1000, 1500, 2000, 3000, 4000\}.$$

Figure 16b illustrates the signal-to-noise ratio  $\text{SNR}(n) = \text{floor}^*/\text{sd}(\widehat{\text{floor}}_n)$ . On FACET, the ratio crosses 1 at about  $n = 450$  and then increases. Although FACET exhibits substantial group-size imbalance, the same detectability pattern is still observed. In particular, group imbalance affects finite-sample variability but does not eliminate the signal itself, which highlights that the trade-off mechanism is intrinsic.

### F.4 Stability under Calibration Resampling

We verify that the trade-off mechanism observed on the FACET dataset is not an artifact of a single calibration split. We keep the model outputs and the test set fixed, and repeat age-stratified calibration subsampling at  $\alpha = 0.1$ . Concretely, we perform 20 repetitions using 70% of the full calibration size. For each repetition, we calculate the key quantities as in Section 5.4.

Table 24 demonstrates that the resampling means remain close to the values with full calibration size. The pooled RMS coverage gap stays near 0.008, the induced RMS set-size gap remains around 0.18, and the equalized set size policy continues to produce a nonzero RMS coverage gap of about 0.019. Therefore, the empirical trade-off pattern in Section 5.4 is stable under repeated calibration perturbations.

## G Computational Resources

All experiments were conducted on a Windows 11 computer with an Intel Core i9-12900H CPU, an NVIDIA GeForce RTX 3080 Ti Laptop GPU (16 GB VRAM), and 32 GB RAM. Each reported experiment was completed within one hour.

Table 23: Configuration for FACET with RAPS.

Setting	Value
Dataset	FACET
Groups	Younger, Middle, Older, Unknown
Labels	20 occupations
Vision-language model	CLIP ViT-L/14
Image preprocessing	bbox crop with 0.08 expansion
Validation samples	4,122
Calibration samples	11,776
Test samples	4,122
Primary target $\alpha$	0.10
RAPS temperature	0.60
RAPS $\lambda$	0.02
RAPS $k_{\text{reg}}$	1
Temperature-perturbed group	Younger
Temperature values	1.0, 1.1, 1.25, 1.5, 1.75, 2.0
Test accuracy / macro-F1	0.6994 / 0.7369

Table 24: FACET stability under calibration subsampling at  $\alpha = 0.10$ .

Metric	Original	Resampling mean $\pm$ sd
Pooled RMS coverage gap	0.0083	0.0085 $\pm$ 0.0005
RMS set-size gap after $q \rightarrow q_g$	0.1717	0.1828 $\pm$ 0.0311
RMS coverage gap after equalized size	0.0199	0.0186 $\pm$ 0.0044